Adv Polym Sci (2016) 274: 241–294
DOI: 10.1007/12_2014_296

Published online: 13 January 2015

Microwave-Assisted Synthesis of Hybrid Polymer Materials and Composites

Dariusz Bogdal, Szczepan Bednarz, and Katarzyna Matras-Postolek

Abstract The fabrication of polymer–inorganic hybrid materials and composites under microwave irradiation benefits from a number of advantages such as reduction in processing time, more uniform heating of materials (i.e., reduced thermal gradient), faster curing of resins, and more efficient crosslinking of composite materials. For polymer hybrid materials, the advantages of microwave-assisted synthesis include smaller particle size, narrower particle size distribution, greater particle density, and higher exfoliation degree, which substantially improve the performance of the final material. A decrease in size of the various components is one of the cornerstones of the push towards improvements in electronic and optical devices, drug delivery, medical scaffolds, biosensors, imaging agents, and analytical technology. This chapter discusses recently published reports on the preparation and characterization of composite materials and polymer hybrids obtained under microwave irradiation using various types of polymer matrix and resins together with inorganic materials such as glass and carbon fibers, carbon black, layered materials (e.g., clays and double hydroxides), metal nanoparticles and nanowires, as well as carbon-based materials (e.g., fullerenes and nanotubes). A survey of past achievements in the preparation of polymer–inorganic hybrid nanocomposites under microwave irradiation can be found in a previously published review paper (Bogdal et al., Curr Org Chem 15:1782, 2011).

Keywords Composites · Hybrid · Inorganic · Microwave irradiation · Polymer

D. Bogdal (✉), S. Bednarz, and K. Matras-Postolek
Cracow University of Technology, Faculty of Chemical Engineering and Technology, 24 Warszawska St., 31-155 Krakow, Poland
e-mail: pcbogdal@cyf-kr.edu.pl

Contents

Abbreviations

2bpy	2,2′-Bipyridine
AAEM	Acetoacetoxyethyl methacrylate
AgNP	Silver nanoparticle
AIBN	Azobisisobutyronitrile
AM	Acrylamide
AP	*p*-Aminophenol
APS	Ammonium persulfate
APTES	γ-Aminopropyltriethoxysilane
BPA	Bisphenol A
BPO	Benzoyl peroxide
CA	2-Carboxyethyl acrylate
Cloisite®	Montmorillonite modified with a quaternary ammonium salt
CMC	Carboxymethyl cellulose
CNT	Carbon nanotube
CTAB	Cetyltrimethylammonium bromide
DDM	Diaminodiphenyl methane
DDS	4,4′-Diaminodiphenyl sulfone
DGEBA	Diglycidyl ether of bisphenol A
DMAc	*N*,*N*-Dimethylacetamide
DMT	Dimethyl terephthalate
DPC	Diphenyl carbonate
EDA	Ethylenediamine
EDMA	Ethylene glycol dimethacrylate
EP	Epoxy resin
F-FFF	Flow-field-flow-fractionation
FGM	Functionally graded materials
HA	Hydroxyapatite
HDPE	High-density polyethylene

HTAB	Hexadecyltrimethyl ammonium bromide
KPS	Potassium persulfate
LDH	Layered double hydroxide
LDPE	Low-density polyethylene
LED	Light-emitting diode
MA	Methyl acrylate
MBA	*N*,*N*′-Methylenebisacrylamide
MC	Microcrystalline cellulose
MMT	Montmorillonite
MROP	Microwave-assisted ring-opening polymerization
MSMA	3-(Trimethoxysilyl) propyl methacrylate
MSTT	Hybrid poly(acrylic)–SiO_2/TiO_2 film
MWCNT	Multiwalled carbon nanotube
Nafion	Copolymer of tetrafluoroethylene and perfluoro-3,6-dioxa-4-methyl-7-octene-sulfonic acid
PAI	Poly(amide-imide)
PAMAM	Polyamidoamine dendrimers
PC	Polycarbonate
PCL	Poly(ε-caprolactone)
PCMA	Polycinnamamide Mg/Al mixed oxide nanocomposite
PDMS	α,ω-Diacrylate poly(dimethyl-siloxane)
VSi-25	
PE	Polyethylene
PEG	Polyethylene glycol
PEMFC	Proton exchange membrane fuel cell
PEO	Poly(ethylene oxide)
PET	Poly(ethylene terephthalate)
PETI-5/IM7	Phenylethynyl-terminated polyimide
PMMA	Poly(methyl methacrylate)
PoPD	Poly(*o*-phenylenediamine)
PP	Poly(propylene)
PS	Polystyrene
PTFE	Poly(tetrafluoroethylene)
PU	Polyurethane
PVP	Poly(vinylpyrrolidone)
RGO	Reduced graphene oxide
ST	Styrene
SWCNT	Single-walled carbon nanotube
TBAB	Tetrabutylammonium bromide
TEMPO	(2,2,6,6-Tetramethylpiperidin-1-yl)oxyl
TIP	Titanium tetraisopropoxide
TMPTA	Trimethylolpropane triacrylate
Tween-20	Polyoxyethylenesorbitan monolaurate
ZSM	Zeolite Socony Mobil
εCL	ε-Caprolactone

1 Introduction

Polymer composites are already well recognized for their improved characteristics in comparison with homogenous polymeric materials [1]. They are extensively used in civil engineering to design and build buildings, bridges, and roads, to strengthen structures, and to cover constructions. About 30% of all polymers produced each year (i.e., 280 million tons in 2011) are used in the construction sector and building industries. Moreover, polymer composites are also used in the transportation, marine, aerospace, biomedical, electronics, and recreation industries. Thus, further improvement in the properties of polymer composites, in addition to improved performance and application, are continually being researched [2]. On the other hand, polymer hybrid materials, which consist of functional inorganic particles or aggregates embedded in a polymer matrix, exhibit a number of intriguing properties that cannot be obtained with organic polymers or inorganic materials independently. For example, polymer hybrids containing nanoparticles were found to be suitable materials for optics and electronics, and have been used to produce devices such as light emitting diodes (LEDs), photodiodes, and photovoltaic cells [3, 4]. Owing to the implementation of simple fabrication processes, tunable size, surface charge, and high loading capacity, polymer hybrids offer numerous advantages in medical applications such as drug delivery [5, 6], scaffolds [7, 8], biosensors [9, 10], imaging agents [11, 12], and analysis [13].

The difference between composites and hybrid materials, according to current terminology, is attributed to interactions of the inorganic particles/aggregates with polymer matrix. A IUPAC technical report defines composites as "multicomponent materials comprising multiple different (non-gaseous) phase domains in which at least one type of phase domain is a continuous phase" [14], whereas elsewhere the notation "the components as well as the interface between them can be physically identified" is added [15]. In contrast to composites, hybrid materials are more difficult to classify because of their differing types and properties. In general, inorganic–organic hybrid materials are classified into two major classes [16]. The first type of hybrid materials are called "class I materials" when inorganic/structural material in the form of particles of varying sizes and shapes are mixed with a polymer matrix and the inorganic particles interact only weakly through hydrogen bonding or van der Waals interactions with the organic/polymer matrix. In class II materials, the organic/polymer and inorganic components are joined through covalent or ionic bonds and no boundaries are indicated at their interfaces [17].

Depending on the size scale of its components and the degree of mixing between the two phases, similarly prepared hybrid materials can exhibit significant differences in composite properties. For example, depending on the cation exchange capacity of layered silicates, three main types of materials can be obtained. First,

when the polymer is not capable of penetrating between the silicate sheets, phase-separated material is prepared with properties similar to traditional microcomposites. Second, when a single polymer chain is able to penetrate between the silicate layers, a well-ordered multilayer morphology results with alternating polymeric and inorganic layers, a so-called intercalated structure. Third, when the silicate layers are entirely and equally distributed in a continuous polymer matrix, an exfoliated structure is formed. In each case, the physical properties of the resultant composite or hybrid polymeric material are significantly different; intercalated and exfoliated composites are often called nanocomposites [18]. Thus, desired polymer composites and polymer hybrids have to be prepared with structural modeling and careful control of components. When the structural configurations of inorganic and organic/polymer components are far from their ideal configuration, the material properties are only the average of the properties of each component, depending on the concentration of each component [17].

The formation of multiphase composites and hybrid materials and associated improvement in properties compared with conventional organic and polymeric materials are not only the result of research in material engineering laboratories. Materials with such functional complexity can also be found in nature, for example, bones, teeth, and teeth enamel (composed of hydroxyapatite and proteins) [19] or the aragonitic nacreous layers of abalone shell [20]. However, at present, most synthetic protocols for preparation of composites and hybrid polymers need high temperature or pressure and very reactive chemicals, whereas these natural materials can be created at ambient temperature and in aqueous environments by biological systems. Therefore, nonconventional methods for the manufacture of polymer hybrids and composites with properties comparable to those of natural materials still have to be elaborated.

During the last three decades, microwaves have been applied in a number of highly useful methods as an efficient energy source during polymer synthesis and processing [21–24]. In addition to the application of microwave irradiation in polymer preparation, these microwave methods are also used for the preparation of polymer hybrids and composite materials [25, 26].

Because of the ability to interact directly with one or more components of composite materials through specific interactions, microwave irradiation offers a number of advantages compared with conventional heating methods. The methods that use microwave irradiation are applied for forming, joining, and bonding polymers and composites. In fact, most polymers are rather transparent to microwave irradiation, which means that they do not absorb enough microwave energy to be heated. However, acceptable microwave heating can be observed in the presence of fillers such as carbon black, graphite, carbon nanotubes (CNTs), clays, silicates, layered double hydroxides (LDHs), metal or metal oxide powders, nanoparticles, nanowires, and conducting polymers [26]. In such processes, microwave irradiation is used to soften and/or thaw thermoplastic polymers, cure monomers and prepolymers, and/or initiate reactions of inorganic particles or aggregates with the polymer matrix.

In this context, the application of microwave irradiation for the preparation of polymer nanoparticles allows control of the size distribution and reduced dispersity of nanoparticles within a shorter reaction time than with conventional heating methods because of more uniform and rapid heating [27]. The possibility of very rapid curing of polymer composites and hybrid materials under microwave irradiation and the formation of unique structures have been presented in a number of reports. A revision of past achievements in the preparation of polymer–inorganic hybrid nanocomposites under microwave irradiation can be found in a previously published review paper [1].

In this chapter, it will be shown that control of such parameters as particle size, particle size distribution, and particle density together with the application of microwave irradiation strongly influence the properties of the obtained materials. For example, a sample of polyamide-6/clay nanocomposite containing 5 wt% of clay had a heat distortion temperature 87°C higher than a plain polyamide-6 reference sample. In addition, the tensile strength and tensile modulus were 49% and 68% higher, while the impact strength did not change [28]. In another example, polyurethane (PU) foams were modified by addition of 5 wt% montmorillonite (MMT) clay during the foaming process, and in comparison with plain PU foams they exhibited increases of 650% and 780% in the reduced compressive strength and modulus, respectively [29].

2 Composite Materials

Regarding the preparation of composite materials, microwaves were investigated as an alternative to conventional heating methods for glass/epoxy laminates [30]. For this purpose, a numerical simulation of the one-dimensional transient temperature profile of the composite materials was elaborated for both microwave and conventional conditions. Bisphenol-F/epichlorohydrin epoxy resin and aromatic diamine as a hardener were applied as substrates. The microwave multimode applicator was a cylindrical cavity (500 L) equipped with multiple microwave inputs and a mode stirrer to ensure homogenous distribution of the microwave power. It was possible to control the cure of the composite materials and improve the properties of thick-section composites by feedback power control and through more efficient energy transfer under microwave conditions in comparison with conventional heating (Fig. 1). The power of microwave irradiation was changed constantly from 0 to 6 kW, which allowed more uniform heating of thick glass/epoxy laminates (25 mm) and eliminated thermal runaway caused by exothermic reactions during curing [30].

Applying differential scanning calorimetry (DSC), the cure kinetics of glass/epoxy composites were analyzed for samples cured under both conventional and microwave conditions [32]. Under conventional conditions, isothermal experiments were conducted at 135–175°C, the kinetic model was developed, and the relation between the degree of cure and time was estimated. For the cure kinetics under microwave conditions, a different approach was required because the cure process

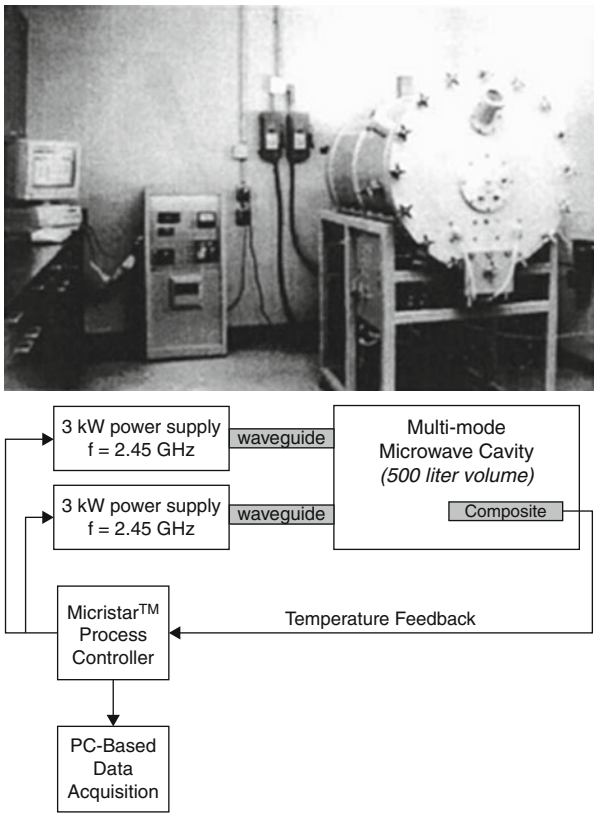

Fig. 1 Multimode microwave reactor with total volume of 500 L (Reprinted from [31] with permission)

was difficult to control in situ within a microwave reactor. Samples placed in the microwave reactor were heated as fast as possible to the desired cure temperature, and the process was finished at a fix time by removing the sample from the reactor and cooling it. For each sample, the residual heat of reaction was measured by means of DSC to evaluate the progress of the cure reaction and conversion of substrates.

Even though thermal gradients were developed during the cure of composite materials under both conventional and microwave conditions, differences in solidification were observed. Under conventional conditions, highest values of the outside-in cure gradients were observed during the early stages of the cure cycle, and the maximum cure rate for the composite materials was noted at the beginning of cure. Both theoretical and experimental data revealed that microwave irradiation initiated an inside-out cure of the thick laminates as a result of volumetric heating, which substantially shortened the total processing time (Fig. 2) [31].

To observe a reasonable inside-out cure effect under conventional conditions, the cycle time needed was almost three times longer than under microwave conditions. Reduced thermal gradients were observed during the early stages of microwave processing, but the desired inside-out cure was successfully developed,

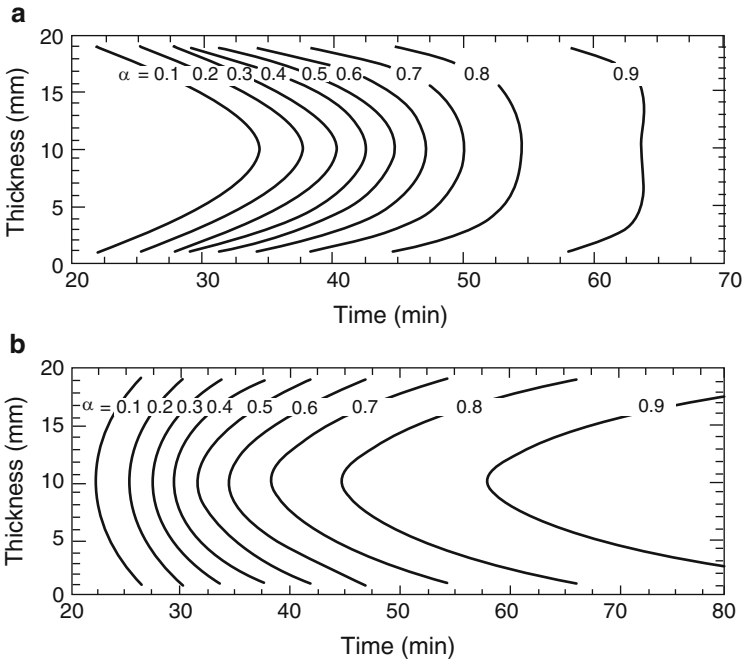

Fig. 2 Formation of cure gradients with two laminates during (**a**) conventional and (**b**) microwave cures (Reprinted from [31] with permission)

which resulted in better control over the solidification behavior of composite materials and reduced the overall processing time [31].

In another report, it was shown that the sample size, amount, and geometry of substrate materials were important parameters during microwave processing. For instance, when the amount of irradiated material was changed from 5 to 15 g, the temperature increased by 32°C in 10 min at the same microwave power. Moreover, the sample of 5 g polyimide resin did not absorb enough microwave energy to be heated efficiently during irradiation, showing that a critical mass was needed to absorb the microwave energy by a substantial amount. Addition of a good microwave absorber (e.g., graphite) strongly increased the absorption of microwave energy by the composite material and resulted in efficient heating (Fig. 3) [33].

It was also shown that, depending on the type of filler (i.e., talc, zinc oxide, and carbon black), the susceptibility of the polymer for microwave absorption during processing was different [34]. The relative temperature rise of high-density polyethylene (HDPE) containing the same amount of various fillers during irradiation with 200 W of microwave power for 1 min is shown in Table 1. Irradiation of neat HDPE with the same power and time gave no significant temperature rise.

As can be expected, carbon black was the most effective filler for increasing microwave absorption of HDPE samples. Moreover, the efficiency of microwave absorption was proportional to the surface area of carbon black; thus, selecting a

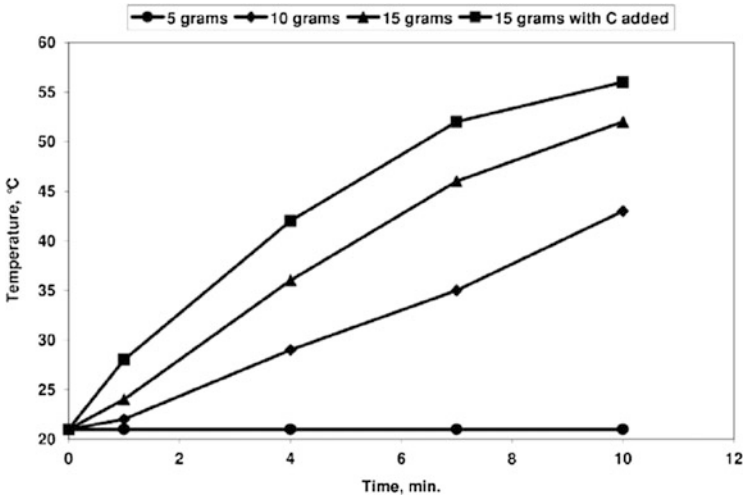

Fig. 3 Effect of sample size on the microwave absorption of undried RP-46 resin (Reprinted from [33] with permission)

Table 1 Relative temperature rise for HDPE at 16% v/v loading of different fillers

Filler	Temperature rise (°C/min)
Carbon black N550	177 ± 10
Zinc oxide	30 ± 5
Talc	3 ± 1

grade with a high surface area is recommended. Relative temperature rise and heat efficiency as a function of carbon black surface area are presented in Fig. 4 [34].

Carbon fibers were also applied as active components, which increased the susceptibility for microwave absorption during processing of phenylethynyl-terminated polyimide composites (PETI-5/IM7). For this purpose, six different microwave cure cycles in the frequency range of 2.4–7.0 GHz and three thermal cycles were carried out. It was found that glass transition temperatures (T_g) were higher for the composites prepared under microwave irradiation in comparison with the composites prepared using the same time–temperature cure cycle under conventional conditions. In addition, microwave-cured composites showed higher shear strength, flexural strength, and modulus than conventionally cured composites, which were often characterized by incomplete crosslinking. It was also shown that under microwave irradiation it was possible to prepare unidirectional polyimide–(carbon fiber) composites with superior thermal and mechanical properties in half the time required for the conventional process (Fig. 5) [35].

For functionally graded materials (FGMs), the composition and structure gradually changes over the volume of the composite materials, resulting in corresponding changes in the mechanical properties of the material, so it is

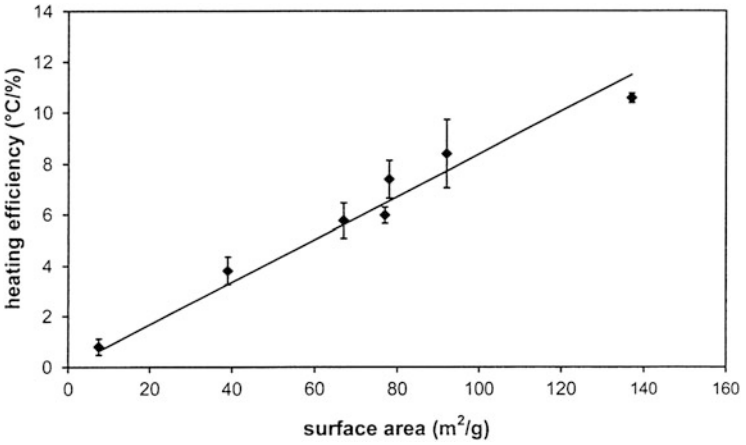

Fig. 4 Relationship between microwave heating efficiency and surface area for carbon black (Reprinted from [34] with permission)

expected that these properties create new functions of the composite materials. The T_g, tensile strength, and modulus (E) of FGMs obtained from an epoxy resin (EP)–polyurethane (PU) elastomer system in the presence of a stoichiometric amount of diaminodiphenyl methane (DDM) as crosslinking agent under microwave irradiation were investigated [36].

In a typical procedure, 65 wt% dichloromethylene solutions of EP/PU/DDM at different ratios of EP to PU were irradiated at 200 W for 20 min in poly(tetrafluoroethylene) (PTFE) molds to form a layer that was submitted for subsequent casting and irradiation. When all the layers were formed, each sample was irradiated at 400 W for 30 min. The obtained composite materials were characterized by T_g and modulus, which varied gradually from −54 to 162°C and from 0.069 to 3.20 GPa, respectively (Table 2) [36].

In the last decade, carbon nanotubes (CNTs) have gained attention because of their unique structure and properties. Because of their remarkable mechanical and electrical properties, CNTs are used as fillers in the fabrication of polymeric composites. Moreover, CNTs show strong microwave absorption with intense heat release and very fast temperature increase [37, 38], although this phenomenon is not yet fully understood. The interaction was explained by dipole polarization induced by the alternating electric field, as well as mechanical vibrations caused by phonon–phonon interactions [39].

Recently, functional CNTs were incorporated on a polyethylene (PE) surface for a microwave welding process [40]. In order to study the interfacial strength of CNT/PE nanocomposites, two layers of CNT films were stacked between a pair of PE strips and welded under microwave irradiation for 30–90 s. For comparison, two PE sheets were compressed and microwave irradiated for the same time. During microwave irradiation, CNT films absorb energy from the microwave field and convert it into heat. The increase in temperature causes localized melting of PE,

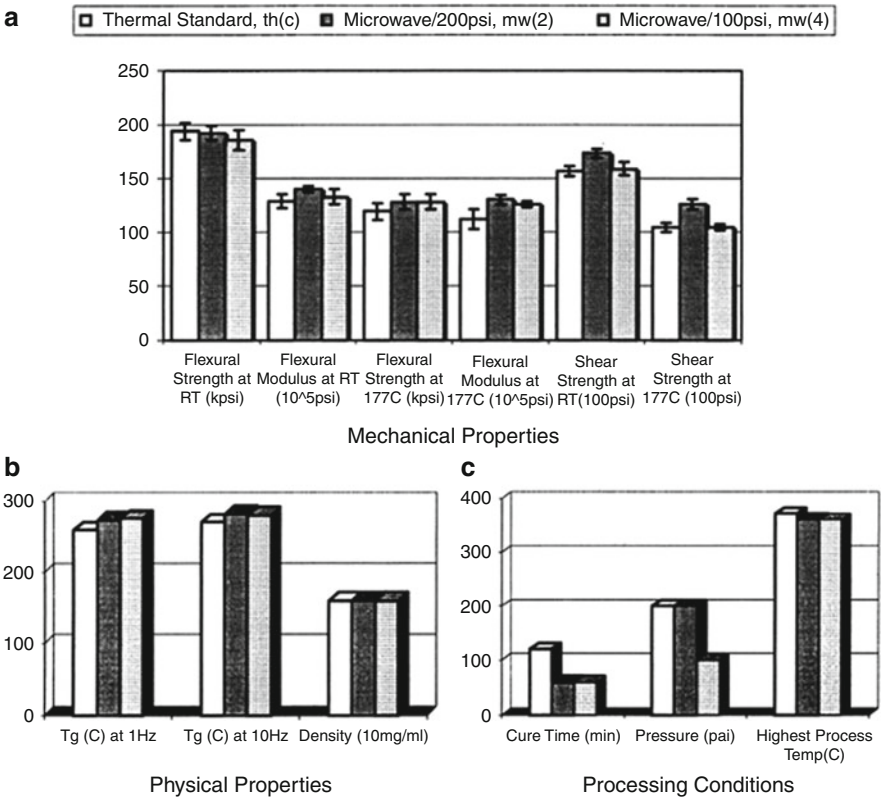

Fig. 5 Comparison of processing conditions and properties of microwave and thermally cured phenylethynyl-terminated polyimide composites (PETI-5/IM7) reinforced with carbon fibers (Reprinted from [35] with permission)

Table 2 Properties along the thickness direction in functionally graded composites of polyurethane and epoxy resin

Sample	PU/EP (w/w)	Tensile strength (MPa)	T_g (°C)	Modulus (E) (GPa)
1	10/0	4.65	−54.0	0.069
2	10/2	5.84	−9.3	0.078
3	10/4	11.6	25.4	0.245
4	10/6	15.2	45.7	0.86
5	10/8	20.8	83.2	0.99
6	10/10	25.8	99.0	1.01
7	8/10	27.4	109.2	1.44
8	6/10	32.5	113.2	1.58
9	4/10	45.8	139.6	2.62
10	2/10	75.9	145.0	2.72
11	0/10	64.8	162.0	3.20

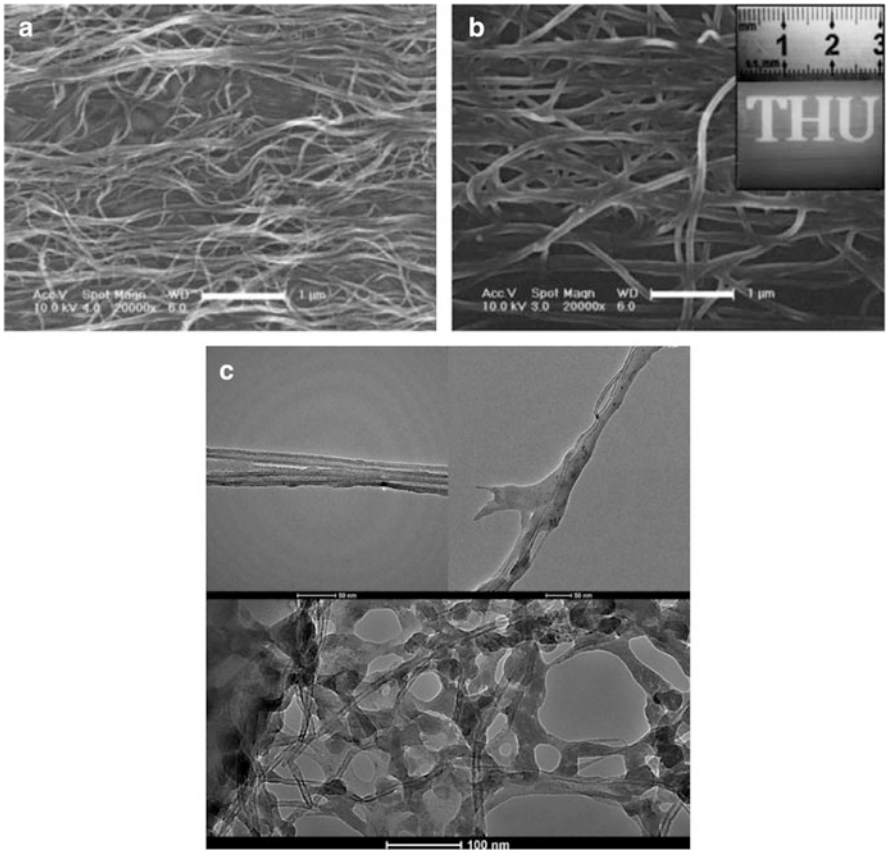

Fig. 6 SEM images of two layers of CNT films on polyethylene surface (**a**) before and (**b**) after microwave welding. (**c**) TEM image of the composite, showing wetting and coating interactions between CNTs and the polymer (Reprinted from [40] with permission)

filling of CNT pores by melted PE, and wetting and wrapping of individual CNTs by the polymer (Fig. 6).

Additionally, the conductive network of CNTs was preserved by the polymer coating. Because of the short processing time, very small amount of CNTs (1.5 μg/cm^2), and taking into account that PE is a microwave-transparent material, the bulk of PE sheets remained at room temperature during microwave welding and thus the polymer structure remained unchanged.

In another report, the preparation of poly(*o*-phenylenediamine)/reduced graphene oxide (PoPD/RGO) composite nanosheets using microwave heating was described and their effective adsorption of lead ions was examined [41]. In a typical synthesis of a hybrid PoPD/RGO composite, a homogenously dispersed mixture of graphene oxide and *o*-phenylenediamine (oPD) in water was placed in a microwave

oven (210 W) for 20 min (Fig. 7). The final product was collected by filtration and washed with water. During the reaction process, graphene oxide nanosheets were used as oxidant to polymerize oPD monomer to form poly(*o*-phenylenediamine) (PoPD) on their surface, while the graphene oxide nanosheets themselves were reduced.

Hybrid PoPD/RGO composites were characterized by transmission electron microscopy (TEM) (Fig. 8), X-ray diffraction (XRD), and X-ray photoelectron spectroscopy (XPS). It was confirmed from TEM images that the microwave-assisted process successfully produced PoPD/RGO composite nanosheets with crumpled morphology. The obtained PoPD/RGO composite materials were tested and evaluated as a potential adsorbent for the removal of lead ions. The study showed that hybrid PoPD/RGO composites exhibited a favorable performance for the removal of lead ions and that the adsorption processes were well fitted by a pseudo-second-order kinetic model [41].

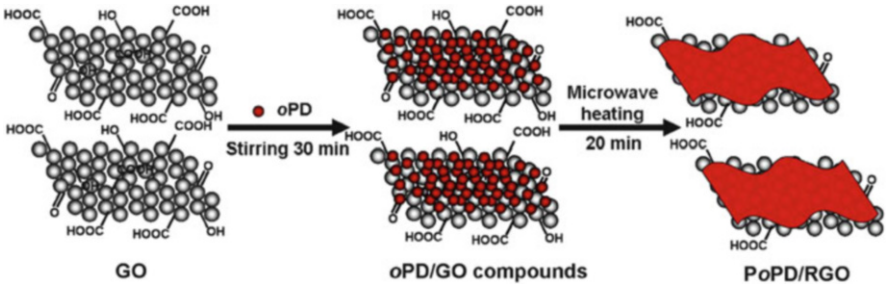

Fig. 7 Fabrication of poly(*o*-phenyldiamine)/reduced graphene oxide (PoPD/RGO) composite nanosheets (Reprinted from [41] with permission)

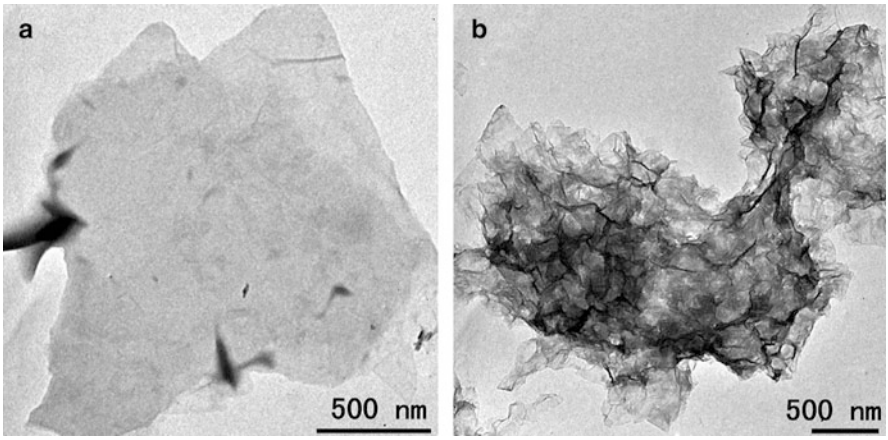

Fig. 8 TEM images of (**a**) graphene oxide; (**b**) poly(*o*-phenyldiamine)/reduced graphene oxide composite nanosheets (Reprinted from [41] with permission)

3 Nanocomposites and Hybrid Materials

Polymer nanocomposites are materials in which inorganic components with an average particle/aggregate size of less than 100 nm are uniformly distributed in an organic polymer matrix; the relative concentration of the inorganic component is only a few percent by weight. Recently, nanocomposites composed of polymer and clay have received considerable interest for the preparation of novel structural and functional materials. Clays and other layered materials (e.g., LDHs) possess the ability to absorb microwave irradiation thanks to the water molecules that are present in the hydration shell of the material interlayer cations. When an inorganic component possesses a well-defined layer and the particles are homogenously distributed in the polymer matrix, the competition between the intragallery polymerization reaction (which takes place between the clay layers) and the extragallery crosslinking of bulk reaction mixture results in two types of composite/nanocomposite structures [42, 43].

3.1 Polycarbonate and Poly(ethylene oxide)

During solid-state polymerization of polycarbonate (PC) prepolymer for the fabrication of PC/MMT nanocomposites under conventional conditions, the reaction temperatures are often too high for organophilic groups in the gallery of MMT to endure during the polymerization [44]. Thus, microwaves were used for the polymerization of PC prepolymer, prepared by melt reaction of bisphenol A (BPA) with diphenyl carbonate (DPC) and intercalated with modified montmorillonite (m-MMT) by melt mixing and solution mixing techniques. The polymerization was carried out in a microwave oven with different irradiation times (6–12 s) at 220°C to afford PC/MMT nanocomposites in the solid state (Fig. 9).

XRD analysis proved that PC/MMT nanocomposites obtained under microwave conditions are characterized by a more homogenous dispersion of MMT silicate in the polymer matrix. Subsequently, WAXD showed that microwave irradiation during solid-state polymerization of PC prepolymers imposed a change in the nanocomposite structure from pre-intercalated into an exfoliated structure. Thus, solid-state polymerization under microwave irradiation was more successful in incorporating a homogenous dispersion of clay into the polymer matrix than polymerization under conventional thermal conditions [44].

Similarly, poly(ethylene oxide) (PEO) nanocomposites with MMT, hectorite, and laponite were obtained by a melting intercalation method under microwave conditions. It was confirmed that PEO chains were interposed between the clay layers to coordinate the interlayer cations (Fig. 10).

Study of the influence of irradiation time and power, and the amount and ratio of the components, on the polymerization reaction showed that it was impossible to obtain an intercalated structure for reaction times shorter than 5 min. For irradiation

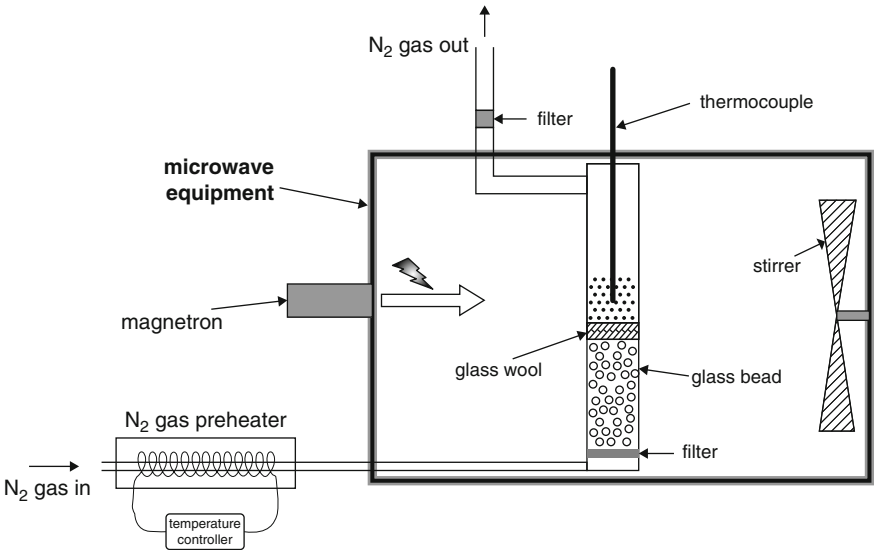

Fig. 9 Microwave equipment for solid-state polymerization (Reprinted from [44] with permission)

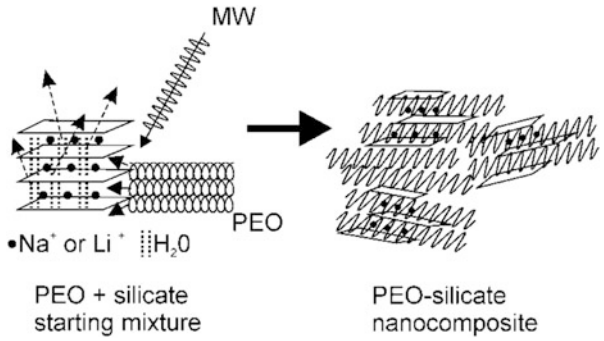

Fig. 10 Scheme of microwave-assisted melt-intercalation reaction (Reprinted from [45] with permission)

times longer than 5 min, XRD patterns proved the PEO intercalation between clay layers, giving interlayer spacing of about 1.8 nm and various degrees of stacking order of the clay particles, which increased with longer irradiation time [45].

Polymer/clay composites can be applied as materials for manufacture of barrier layers for packaging [46]. Recently, poly(ethylene-*co*-vinyl acetate)/clay nanocomposites were prepared by solution intercalation under microwave irradiation [46]. A solution of copolymer in THF was mixed with MMT clay (Bentone 105) dispersed in toluene and irradiated for various times (5–15 min) at 80 or 135°C in a microwave reactor. Films were prepared by casting the mixture on Petri dishes

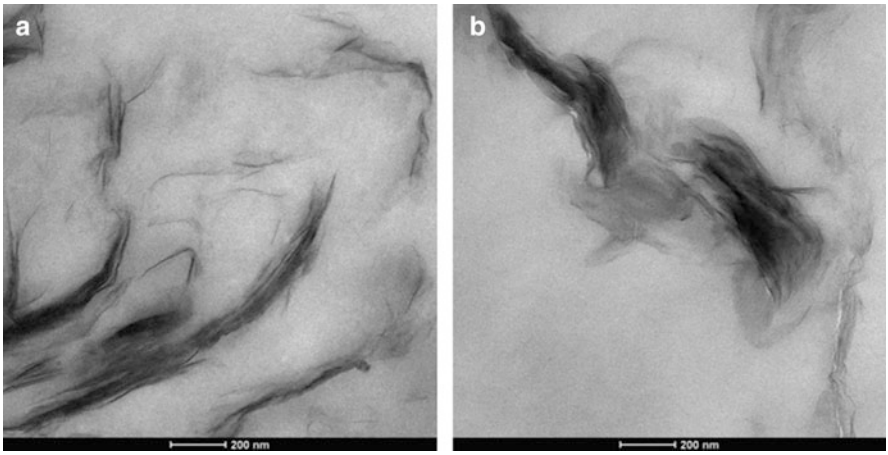

Fig. 11 TEM images of poly(ethylene-*co*-vinyl acetate)/montmorillonite nanocomposites containing (**a**) 1 wt% and (**b**) 10 wt% clay prepared under microwave irradiation. (Reprinted from [46] with permission)

and drying. XRD data for the nanocomposites proved the intercalation process (increase in interlayer spacing) and also indicated no influence of microwave processing on the polymer/clay dispersion degree. These results were in a good agreement with the TEM data (Fig. 11), proving that the clay formed aggregates and that exfoliation was impossible at higher concentrations of inorganic material.

3.2 Poly(ε-caprolactone)

It was shown that poly(ε-caprolactone) (PCL)/clay nanocomposites have a number of enhanced properties in comparison with neat PCL [47–49]. PCL/MMT nanocomposites were prepared by microwave-assisted ring-opening polymerization (MROP) of εCL in the presence of either unmodified or modified MMT in 60 min [50]. In the case of unmodified MMT (Cloisite®Na^+), PCL/MMT nanocomposite with a number-average molar mass (M_n) of approximately 60,000 g/mol was prepared and exhibited an intercalated structure. In turn, applying MMT modified with an alkylammonium salt (Cloisite®30B) resulted in PCL/MMT nanocomposites with a predominately exfoliated structure, with M_n of PCL in the range of 16,300–66,100 g/mol for 0.5–5 wt% of MMT in the composite (Table 3).

Subsequent reports described MROP of εCL with Cloisite®30B as the nanofiller and catalyzed using either tin(II) 2-ethylhexanoate [$Sn(Oct)_2$] or zinc powder. The mechanical properties of PCL/Cloisite®30B nanocomposites were examined. Applying microwaves at 680 W for only 30 min, PCLs with high weight-average molar weight (M_w) of 124,000 and 92,300 g/mol were obtained in the presence of $Sn(Oct)_2$ and zinc powder, respectively [51]. The PCL/Cloisite®30B

Table 3 Ring-opening polymerization of ε-caprolactone

Heating	Filler type	Concentration (wt%)	Temperature (°C)	Conversion (%)	M_n (g/mol)	Polydispersity index
Microwave irradiation	30B	0.5	120	98	66,100	1.5
	30B	3	120	97	34,800	1.7
	30B	3	100	93	43,900	1.5
	30B	5	120	95	16,300	1.8
	Na^+	3	120	98	60,400	1.5
	–	0	120	85	44,300	1.7
Thermal (oil bath)	Na^+	3	120	1	1,000	1.1
	30B	3	120	1	1,300	1.2
	–	0	120	17	6,500	1.1

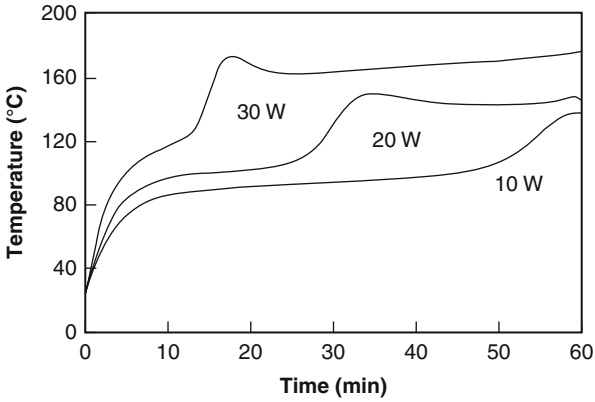

Fig. 12 Temperature–time profiles of polymerization mixture (ε-caprolactone, 0.5 wt% Cloisite®30B as nanofiller and 0.1 mol% Sn $(Oct)_2$ as catalyst) at different power levels (Reprinted from [52] with permission)

nanocomposites possessed a predominantly exfoliated structure. It was concluded that the power of microwave irradiation had a significant influence on the yield and M_w of PCL (Figs. 12 and 13) [51, 53].

3.3 Poly(ethylene terephthalate)

Layered double hydroxides (LDHs), known as anionic clays or hydrotalcite-like compounds, find application in catalysis, adsorption processes, and preparation of composite materials [54, 55]. In situ polymerization of poly(ethylene therephthalate) (PET)/LDH nanocomposites was performed under microwave irradiation [56]. LDHs were treated with dodecyl sulfate prior to the synthesis to improve compatibility between PET and LDHs and dispersed for 1 h in an ultrasonic bath in ethylene glycol prior to the reaction. Then, in considerably reduced reaction time compared with the conventional process, the polymer nanocomposites were prepared under reflux conditions by mixing 0.05 mol ethylene glycol, 0.25 mol dimethyl terephthalate (DMT), and 0.01 g zinc acetate as catalyst under microwave irradiation. The polymerization temperature was increased to 140°C (20°C/min), then to 200°C (12°C/min), and finally to 270°C and maintained for 35 min. Eventually, nanocomposites (1, 2, 5, and 10 wt% LDH) with uniformly dispersed and exfoliated LDHs in the polymer matrix were prepared. Nanocomposites with low concentration of LDH were thermally more stable than neat PET (Fig. 14).

Exfoliation and dispersion was complete for LDHs at 5 wt%; higher concentrations resulted in LDH aggregates in the nanocomposite. Moreover, compared with conventional processes, curing of the nanocomposites under vacuum can be avoided because it neither modifies the structure or properties of the nanocomposites nor enhances the thermal stability [56].

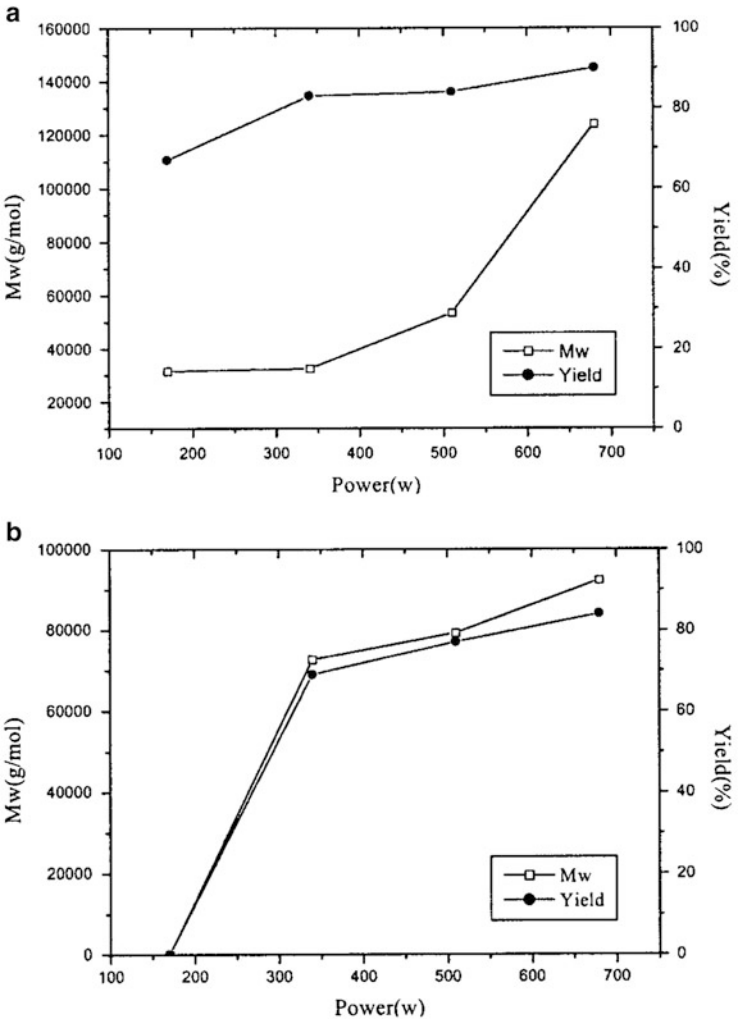

Fig. 13 Effect of irradiation power on polymerization of poly(ε-caprolactone): (**a**) 0.1% $Sn(Oct)_2$ as catalyst, 30 min reaction time; (**b**) 1% zinc powder as catalyst, 270 min reaction time (Reprinted from [51] with permission)

3.4 Epoxy Resins

The synthesis of epoxy/MMT nanocomposites in the presence of silicone acrylate (α,ω-diacrylate poly(dimethyl-siloxane), PDMS V-Si21) under microwave irradiation has been described together with the effect of different clay modifiers [57]. The epoxy/MMT nanocomposites were prepared using MMT previously modified by dodecyl-, hexadecyl-, and octadecylamines or hexcadecyltrimethyl ammonium

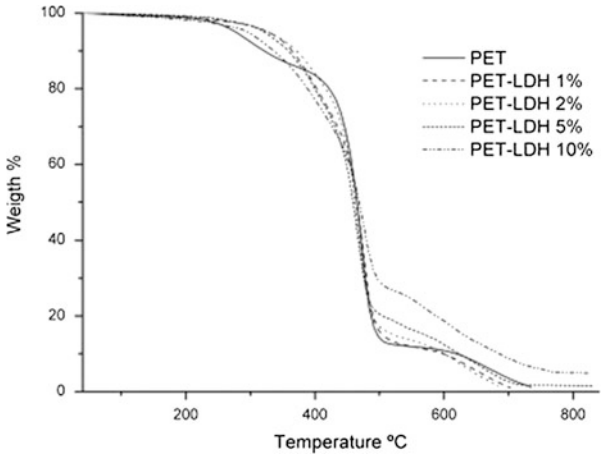

Fig. 14 Thermogravimetric curves for PET and PET-LDH nanocomposites (Reprinted from [56] with permission)

bromide (HTAB). Physical activation of MMT before reaction with ammonium salts led to exfoliation of clay in the polymer matrix and also prevented agglomeration, resulting in a uniform structure [57]. The organoclays (3 and 5 wt%) were stirred with a BPA-based epoxy monomer at 80°C for 30 min and then 50 wt% of polyamine hardener was added to the epoxy resins. The mixture was poured into a mold and irradiated in a microwave reactor for 20 min at 400 W power. To obtain siloxane-modified samples, 5 or 10 wt% PDMS V-Si21 was mixed with the epoxy resins before addition of the hardening agent.

Epoxy/MMT nanocomposites containing HTAB-modified clay were characterized by better mechanical properties than those with dodecyl-, hexadecyl-, and octadecylamines. It was found that the modulus (E) increased, with a corresponding decrease in toughness, with an increase in MMT content; however, an increase in PDMS V-Si 21 concentration resulted in the opposite effect. For each sample containing 5 wt% of MMT and 5 wt% of PDMS V-Si 21 (samples "8 Dodecylamine" and "8 HTAB" in Table 4), in which interlayer spacing was increased, the modulus was as high as that of neat epoxy (sample no. 1) but toughness was greater than that of neat epoxy. In such a way, the mechanical properties of samples containing MMT and PDMS V-Si 21 were improved (Table 4) [57].

Another paper describes the application of a microwave-assisted protocol for the fabrication of CNT/epoxy nanocomposites with a very high dielectric constant and low dielectric loss [58]. Multiwalled carbon nanotubes (MWCNTs) of average diameter <10 nm and length of 5–15 μm were blended at 65°C with diglycidyl ether of bisphenol A (DGEMA) and an imidazole derivative as polymerization catalyst. Next, the mixture was cast into a mold and pre-cured under microwave irradiation (700 W) for 2 min in six cycles, followed by post-curing in a thermal oven at increasing temperature from 80 to 150°C for total time of 10 h. For

Table 4 Mechanical characterization of nanoparticle samples containing modified clays

Sample no.	Young's modulus (E) (MPa)	Maximum strength (σ_{max}) (MPa)	Strain at maximum force (F_{max}) (%)	Strength at break (MPa)	Strain at break (%)	Toughness (W) at break (J)
1[a]	1,433	34.0	6.0	23.5	11	0.60
8 Dodecylamine[b]	1,278	25.5	3.9	21.6	12	0.88
8 HTAB[c]	1,391	33.4	5.1	25.6	12	1.10

[a]Neat epoxy
[b]Epoxy containing 5 wt% dodecylamine and 5 wt% PDMS V-Si 21
[c]Epoxy containing 5 wt% HTAB and 5wt% PDMS V-Si 21

comparison, a series of composites was produced under conventional heating at similar curing parameters (temperature and time). Electrical conductivities and dielectric properties of the resulting composites were studied as a function of the MWCNT content (0.05–0.5 vol%) and method of curing (microwave versus thermal). Based on those investigations, it was suggested that, compared with thermally cured composites, MWCNTs in composites prepared under microwave conditions create uniform connecting paths and thus form a conducting network above the percolation threshold of the filler. Additionally, dielectric spectroscopy studies indicate that MWCNTs in composites cured under microwave conditions not only have better dispersion but also align in one direction, resulting in lower dielectric loss of the material. Microwave curing of MWCNT/epoxy composites allows the development of novel materials with high dielectric constant and low dielectric loss, which are very important for the electronic and power industries.

In another report, a microwave protocol was developed to reduce graphite oxide to graphene, which is used as a conductive additive in epoxy composites [59]. The reduction of graphite oxide at the gram scale was performed in a microwave oven operated at 1,000 W of microwave power. As confirmed by XRD studies and elemental and Fourier transform infrared (FTIR) analysis, 2–3 min of microwave irradiation was sufficient to obtain graphene. The work demonstrates that addition of only 0.3 wt% of graphene increases the electrical surface resistivity of the nanocomposite, which makes graphene/epoxy materials useful for batteries, electrodes, electromagnetic interference shielding materials, antistatic coatings, sensors etc.

3.5 Acrylic Resins

Microwave-assisted synthesis of polymeric/inorganic hybrid nanocomposites for encapsulation of photoelectronic devices has also been described [60, 61]. Several organic/inorganic composites have been fabricated under microwave conditions, for example, acrylic/alumina (Fig. 15a), polyurethane–acrylic/alumina (Fig. 15b), silicone–acrylic/alumina (Fig. 15c), silicone–polyurethane–acrylic/alumina

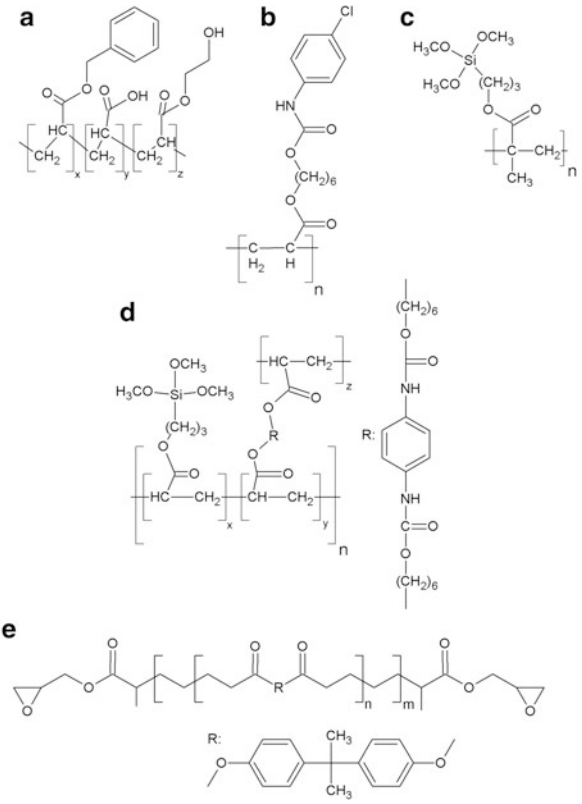

Fig. 15 Synthesis of series of nanocomposites under microwave irradiation: (**a**) acrylic/alumina, (**b**) polyurethane–acrylic/alumina, (**c**) silicone–acrylic/alumina, (**d**) silicone–polyurethane/acrylic/alumina, and (**e**) acrylic/epoxy/mica/boron nitride

(Fig. 15d) [60], and acrylic–epoxy/mica/boron nitride (Fig. 15e) [61]. Alumina, mica, and boron particles of average diameter 30–100 nm, 1–10 μm, and 1 μm, respectively, were used as filler. With microwave irradiation, fabrication of the composites takes only 10 min, in contrast to conventional heating where the polymerization takes 8–24 h. Moreover, microwave-assisted synthesis yielded products with highly reproducible properties. The obtained composites with good adhesive strength, fast curing speed, moderate hardness, high refractive index, and excellent gas resistance were successfully applied for encapsulation of photoelectric devices (LED, OLED) [60]. Additionally, acrylic–epoxy/mica/boron nitride nanocomposites with gas barrier and heat dissipating capacities, were used to protect a top-emitting organic light-emitting diode (OLED) and prolong its lifetime.

In another report, microwave irradiation was applied for the preparation of silver nanoparticles (AgNPs) dispersed in methacrylate monomers. The silver particles possessed a narrow size distribution of 1.0–5.5 nm, with a mean diameter of 2.8 nm. Compared with conventional conditions, the microwave-assisted synthesis of AgNPs proceeded more uniformly to achieve full conversion of reagents at the same time in the whole reaction vessel. Consecutive polymerizations of the

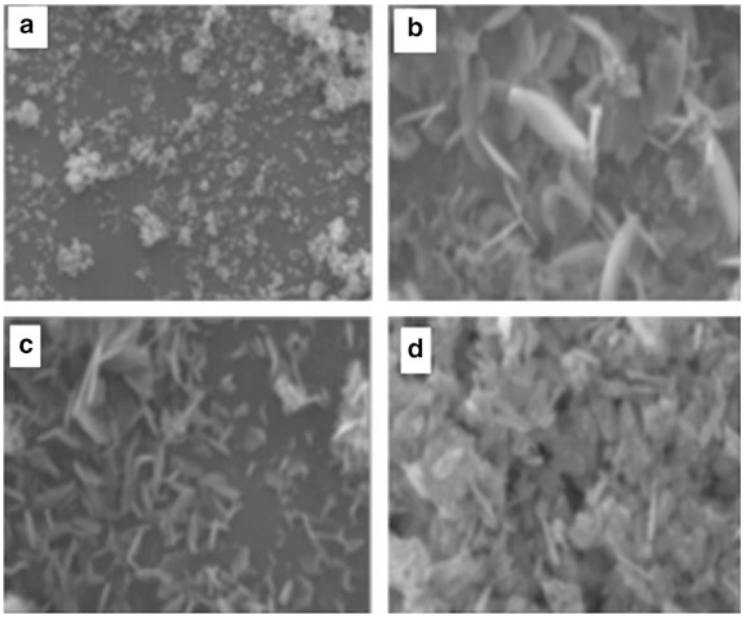

Fig. 16 SEM images of ZnO nanoparticles prepared by the microwave method: (**a**) uncapped and using (**b**) PEG 300, (**c**) PVP, or (**d**) CTAB as capping agent (Reprinted from [63] with permission)

monomers with AgNPs produced silver nanoparticles dispersed in a polymer matrix [62]. In a typical procedure, $C_{13}H_{27}COOAg$ powder (0.634 g) was stirred with cyclohexyl methacrylate (10.0 g) containing triethylamine (NEt_3, 0.191 g) and the mixture irradiated for 5 min at 140°C. Then, photoinitiator (1 wt% of Irgacure 9) was added and the solution spread onto a slide glass substrate. Films were polymerized for 30 min under UV light.

Recently, a microwave technique was used for the preparation of various morphological ZnO nanocrystallites for poly(methyl methacrylate) (PMMA) and PMMA/PU polymer matrices [63]. This work compared reflux and microwave heating methods of synthesis of ZnO nanoparticles. In both cases, poly (ethyleneglycol) (PEG 300), poly(vinylpyrrolidone) (PVP), and cetyltrimethylammonium bromide (CTAB) were used as capping agents. It was observed that, in the case of microwave irradiation, ZnO nanoparticles presented a very wide size distribution for various capping agents compared with the reflux method (Fig. 16). Under microwave irradiation, ZnO nanocrystals were obtained with different morphologies (spherical clusters, one-dimensional sheets, flakes, and platelets) and with cluster sizes between 50 and 400 nm.

ZnO nanoparticles with different morphologies were then incorporated into PMMA and PMMA/PU matrices and ZnO/PMMA nanocomposite films of 0.04 mm thickness prepared by the solution-casting method (Fig. 17). In both cases, the content of ZnO nanocrystallites in the polymer matrix was 0.1 wt%.

Fig. 17 Photographs of ZnO/PMMA and ZnO/PU/PMMA sheets (Reprinted from [63] with permission)

By near infrared reflectance (NIR) and UV-vis spectra analysis of ZnO/PMMA and ZnO/PMMA/PU nanocomposites it was shown that addition of inorganic ZnO nanoparticles into a PMMA matrix significantly improved NIR reflectance efficiency compared with pure PMMA. For instance, neat PMMA had low reflectance of only 2% whereas ZnO/PMMA nanocomposites had increased NIR reflectivity of about 55% at a wavelength of 1,100 nm.

Additionally, the NIR reflectance was investigated and correlated with ZnO particle size and morphology. It was found that the morphology of ZnO plays a key role in obtaining a high NIR reflecting property. The best result (about 55% at 810 nm) was achieved using ZnO nanosheets obtained with PEG 300 capping under microwave irradiation. Taking into account the properties of the obtained ZnO/PMMA nanocomposite, these materials can find potential application as solar thermal control interface films [63].

Poly(acrylic)/SiO_2/TiO_2 (MSMA–SiO_2/TiO_2) core–shell nanoparticle hybrid thin films were also prepared under microwave conditions [64]. The procedure was a combination of the sol–gel reaction, thermal polymerization, and spin coating. First, the colloidal SiO_2–TiO_2 core–shell nanoparticles with OH groups on the surface were prepared, in which uniform layers of titania were deposited by controlled hydrolysis of tetrabutoxyltitanium (6–9 g) in the presence of colloidal silica particles. Then, the coupling agent 3-(trimethoxysilyl) propyl methacrylate (MSMA), colloidal SiO_2–TiO_2 core–shell nanoparticles, deionized water, and THF were mixed in various proportions (Table 5) and the hydrolysis/condensation reactions carried out under microwave irradiation at 60°C for 5–40 min to obtain the MSMA–SiO_2/TiO_2 colloidal solution. In order to obtain hybrid poly(acrylic)–SiO_2/TiO_2 films (MSTT), the colloidal MSMA–SiO_2/TiO_2 was subsequently mixed with a homogeneous THF solution of bifunctional acrylate of ethylene glycol dimethacrylate (EDMA) and a trifunctional acrylate of trimethylolpropane triacrylate (TMPTA) and benzoyl peroxide (BPO) as initiator. The polymerization reactions were run at 60°C for another 5–40 min under microwave irradiation. Then, the reaction solution was spin-coated on a 6-inch silicon wafer and the coated thin films cured on a hot plate.

Table 5 Monomer composition and properties of the hybrid thin films MSTT0–MST100 prepared under microwave irradiation

	MSTT0	MSTT20	MSTT50	MSTT80	MSTT100
Composition					
Core–shell SiO_2–TiO_2 (wt%)	0	20	50	80	100
MSMA (wt%)	25	20	13	5	0
TMPTA (wt%)	45	36	22	9	0
EDMA (wt%)	30	24	15	6	0
Properties					
h (nm)[a]	189	115	111	107	195
n_{633}[a]	1.525	1.601	1.694	1.791	1.870
k_{633}[a]	0.001	0.003	0.006	0.007	0.003
R_a (nm)[b]	0.518	0.794	1.163	1.108	2.017
R_a/h (%)[b]	0.274	0.690	1.047	1.035	1.034
R_q (nm)[b]	0.676	0.853	1.202	1.129	2.114
R_q/h (%)[b]	0.357	0.741	1.082	1.055	1.084
T (°C)[c]	350	247	232	233	–
TGA residue (wt%)[d]	9.14	38.72	64.40	81.72	99.28
TGA residue (wt%)[e]	6.06	24.85	53.03	81.21	100

[a]Thickness (h), refractive index at 633 nm (n_{633}), extinction coefficient at 633 nm (k_{633}) measured by ellipsometer
[b]Roughness (R_a arithmetic mean roughness, R_q quadratic mean roughness) measured by AFM
[c]Thermal glass transition and decomposition temperature measured by DSC
[d]Wt% of residue after thermogravimetric analysis
[e]Wt% of residue estimated from theoretical calculation

Although the particle content reached 90 wt%, SEM analysis of hybrid MSTT-90 thin films showed that the SiO_2–TiO_2 core–shell nanoparticles were homogenously dispersed in the polymer matrix. The particles kept their original size of 15–20 nm, indicating that there had been no particle growth or serious aggregation of the core–shell nanoparticles during the curing procedure. The extinction coefficients (k) of all the MSTT films were almost zero at 190–900 nm, and the films possessed high optical transparency in the UV and visible regions, which indicates that the particle size in the hybrid films was small enough to avoid significant light scattering loss (Table 5).

Finally, comparing the overall reaction times under microwave and conventional conditions, it was found that microwave-assisted synthesis of poly(acrylic)/SiO_2–TiO_2 hybrid materials can be carried out faster (5–40 min) than by the conventional method (1–3 h) [64].

Silver nanoparticles have also been encapsulated in poly-*N*-isopropylacrylamide/acrylic acid microgels [65]. Poly-*N*-isopropylacrylamide/acrylic acid microgel particles crosslinked by *N*,*N*′-methylene bisacrylamide were prepared by surfactant-free emulsion polymerization. Next, microgel dispersion was soaked in aqueous $AgNO_3$ and glucose, and the mixture irradiated in a microwave oven for 15 s (Fig. 18). The resulting microgel-stabilized AgNPs had an average diameter of

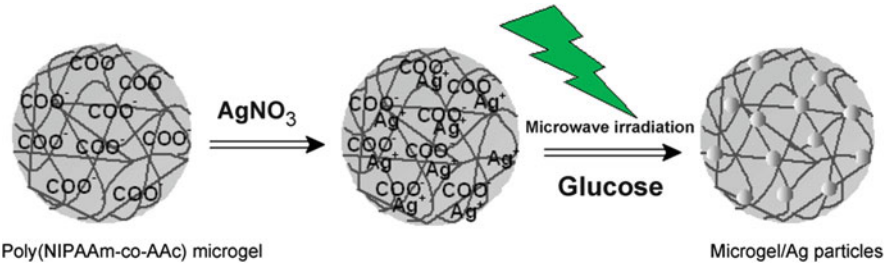

Fig. 18 Microwave-assisted encapsulation of silver nanoparticles in copolymeric microgel (Reprinted from [65] with permission)

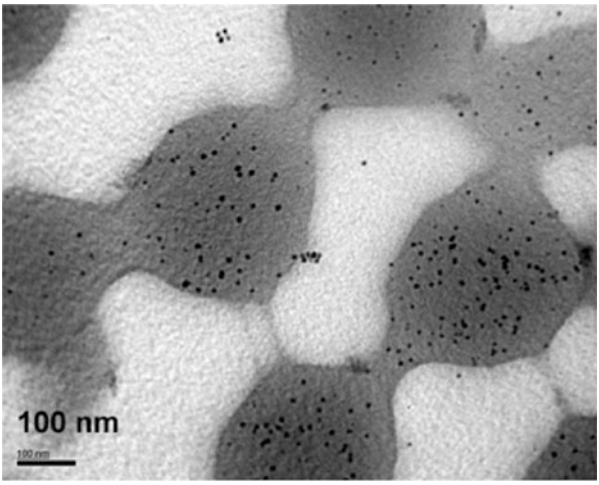

Fig. 19 TEM image of microgel–silver particles after 8 months of storage (Reprinted from [65] with permission)

8.5 nm (Fig. 19) and were stable with negligible aggregation for more than 8 months at room temperature.

In another report, the microwave technique was used for curing hybrid nanocomposite coatings based on an acrylic modified silane (methacryloxypropyltrimethoxysilane) (SiO_2) and TiO_2 nanoparticles. The hybrid nanocomposite coatings were made by the sol–gel method and deposited on a polycarbonate (PC) plate by dip coating. The TiO_2 nanofilaments were added to acrylic modified silane to increase the absorption of microwaves during the microwave-assisted curing process. Finally, the obtained coatings were cured by different methods such as thermal, microwave, and ultraviolet radiation, independently as well as in a combination of microwave and UV methods. Microwave curing was carried out using a 1,000 W microwave oven at the maximum power setting for 2 min. In the case of thermal curing, the samples were thermally treated at 130°C for 4 h. UV

curing was carried using a 3 m medium-pressure mercury lamp (120 W/cm with total wattage/lamp of12 kW) for 4 min. It was found that all the samples possessed very good optical properties and the visible light transmittance of all increased by 1% compared with neat PC film. It was also demonstrated that only the thermal method or a combination of microwave and UV treatment (MW + UV) caused an increase in pencil scratch hardness of samples (3H and 2H, respectively). Moreover, the dual curing process (MW + UV) seemed to be a very good alternative to thermal curing because of substantial time saving for the curing process and significant enhancement of the mechanical properties of samples [66].

Microwave irradiation was also applied for synthesis of poly(acrylic)/TiO_2 hybrid nanocomposite thin films with excellent optical properties [67]. In this study, colloidal TiO_2 nanoparticles stabilized with MSMA were synthesized using a hydrolysis/condensation process under microwave heating at 60°C. Resultant TiO_2 nanoparticles were then polymerized with an acrylic monomer and initiator under microwave irradiation to form a hybrid polymer solution. In this work, three different types of acrylic monomers were used: a single functional acrylate of methyl methacrylate (MMA), a bifunctional acrylate of ethylene glycol dimethacrylate (EDMA), and a trifunctional acrylate of trimethylolpropane triacrylate (TMPTA). The content of TiO_2 nanoparticles in acrylic monomer was changed from 0 to 100%. The thin films of poly(acrylic)/TiO_2 with different content of TiO_2 nanoparticles were spin-coated on a 6-inch silicon wafer. Poly(acrylic)/TiO_2 thin layers were characterized with respect to structure, morphology, and thermal and optical properties (Fig. 20). It was demonstrated that poly(acrylic)/TiO_2 hybrid thin films, even with a very high content of TiO_2 nanoparticles, have excellent optical properties and can be used as antireflection coatings for a various optical devices. Poly(acrylic)/TiO_2 hybrid thin films with the highest content of TiO_2 nanoparticles (90 wt%) had a refractive index n of 1.920. Additionally, optically highly transparent poly(acrylic)/TiO_2 hybrid three-multilayer film showed reflectance of less than 0.5% in the visible range [67].

In a later report, microwave-assisted synthesis of acrylic acid-based hydrogels containing AgNPs was described [68]. Simultaneous formation of a polymeric network by polymerization-crosslinking of acrylic acid with *N*,*N*′-methylenebisacrylamide in aqueous solution and preparation of AgNPs in situ by reduction of $AgNO_3$ led to nanocomposites with potential biomedical applications. The nanoparticles with average diameter of 10 nm were entrapped in polymeric matrix and it was found that the concentration of nanoparticles influenced the swelling capacity of the hydrogels.

3.6 Poly(vinyl carbazole) and Poly(carbazole)

Metal nanostructures have been extensively studied because of their use in applications such as catalysis, optics, electronics, optoelectronics, biological and chemical sensing, and surface-enhanced spectroscopy. Composites with nanocrystals are

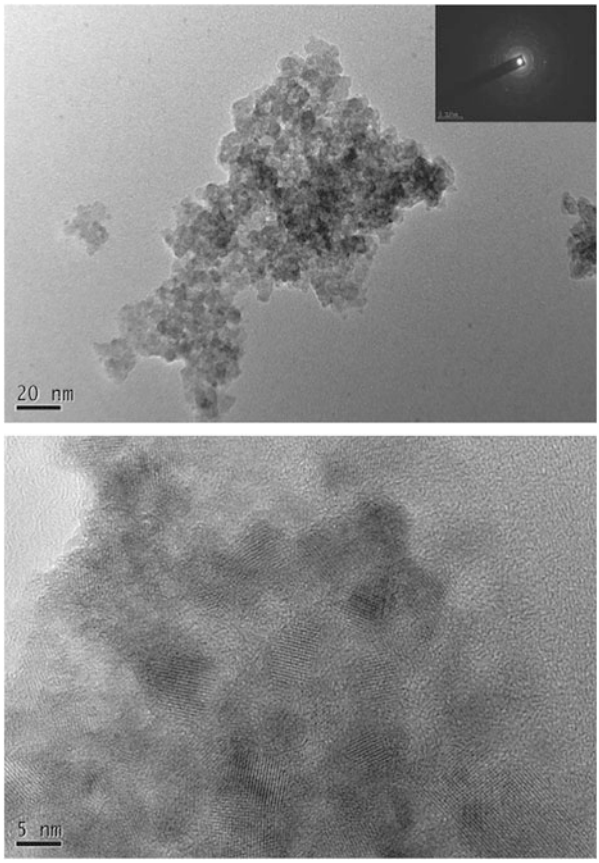

Fig. 20 TEM image and selected area electron diffraction (SAED) pattern of poly(acrylic)/TiO_2 hybrid material with 90% content of TiO_2 nanoparticles (MTT90) (Reprinted from [67] with permission)

obtained by two methods: nanocrystals can be dispersed in a polymer matrix or can be prepared in situ in a polymer. For example, semiconductor–polymer nanocomposites of poly(vinylcarbazole) with nanocrystalline CdS were prepared under microwave conditions in pyridine as solvent. This solvent promotes the polymerization of *N*-vinylcarbazole in the presence of AIBN and formation of CdS nanocrystals from thiourea and cadmium acetate. The reaction mixtures were irradiated in a microwave reactor at 300 W for 5 min under nitrogen atmosphere. It was found that polymerization and formation of the crystalline inorganic salt nanoparticles progressed simultaneously. Thus, in this one-step method it was possible to obtain nanocomposites with uniformly dispersed nanocrystals in a polymer matrix [69].

Nanostructured poly(carbazole) was synthesized within bentonite clay galleries through solvent-free one-pot microwave-assisted reaction [70]. Mixtures of bentonite clay, carbazole, and ammonium persulfate (APS, oxidant) were irradiated for 2–6 min in a microwave oven. The temperature of the process was set at 30, 40, or 50°C. Then, the nanohybrids obtained were thoroughly purified by washing in

solvents. The effect of temperature and time of irradiation on the polymerization yield and morphology of poly(carbazole) nanoparticles formed in the inorganic matrix were studied and the spectroscopic characteristics of nanocomposites examined (UV–vis absorption and fluorescence). Based on thermogravimetric analysis (TGA), it was found that the hybrid materials contained 25–30% of carbazole polymer intercalated in the interlayer space of bentonite. Additionally, the polymer formed particles that ranged in size from 50 to 500 nm. The nanocomposites showed characteristic absorption spectra with three maxima at 250, 450, and 750 nm. They also exhibited blue fluorescence by a main maximum in the 450 nm region. These optical properties make poly(carbazole)/bentonite nanocomposites interesting materials, with potential application in LED and solar cell technologies.

In another work [71], the research focused on microwave-assisted solvent-free synthesis and properties of poly(carbazole)/clay composites. It was found that utilization of different oxidants to persulfate (i.e., benzoyl peroxide and hydrogen peroxide) influenced the molecular weight and morphology (size of nanoparticles) of the polymer formed in bentonite galleries.

Similarly, microwave irradiation was applied for solid-state in-situ polymerization and intercalation of poly(carbazole) between bentonite layers [72]. Mixtures of the clay, carbazole, and ferric chloride (oxidant) with 1:1, 1:0.5, and 1:0.25 weight ratios were irradiated in a microwave oven for 180 s at 35°C. During heating, the oxidant enters bentonite galleries through a cation-exchange process and carbazole molecules diffuse into the basal spacing of the clay where polymerization occurs. The nanocomposites obtained were purified by washing with water and methanol and dried. For some investigations, poly(carbazole) present in the clay galleries was extracted by hot methanol. The results obtained using FTIR, UV-vis, XRD, fluorescence microscopy, and TEM confirmed intercalation as well as polymerization of carbazole in the bentonite galleries. Moreover, at lower poly(carbazole) loading, the macromolecules were oriented transversely and distributed discretely in the clay. In contrast, at higher loading, polymer chains were entangled with each other and probably oriented longitudinally in the narrow space of the clay galleries. TEM images (Fig. 21) of the polymer extracted from the nanocomposites show that poly (carbazole) forms in interlamellar space fibers or organizes to produce cucumber-shaped structures. The results also reveal that the nanocomposites with a small amount of the polymer, due to specific macromolecule organization, show significant fluorescent properties, making the nanocomposite useful for production of fluorescence probes or electronic devices.

3.7 Poly(tetrafluoroethylene) and Nafion

Carbon black-supported poly(tetrafluoroethylene) (PTFE/C) nanocomposites were synthesized by an intermittent microwave irradiation (IMI) method for polymer electrolyte fuel cells, using PTFE emulsion as the precursor [73]. During preparation of the nanocomposite, Vulcan XC-72 carbon black (4.0 g) was added to

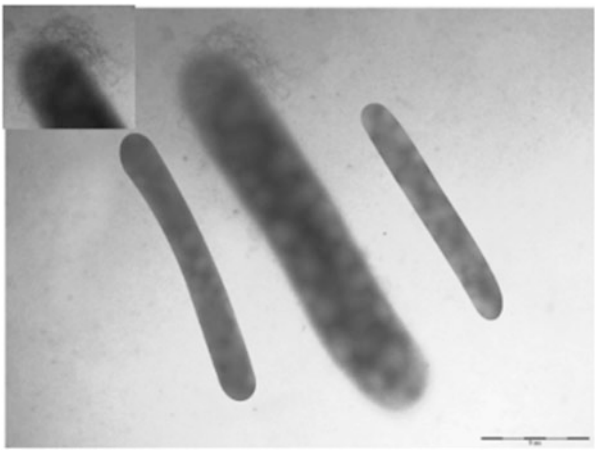

Fig. 21 TEM image of poly(carbazole) extracted from bentonite/poly (carbazole) composite (Reprinted from [72] with permission)

Table 6 PTFE loading and BET surface area of PTFE/C nanocomposites synthesized under microwave irradiation (three bursts of 15–30 s duration)

PTFE/C composite	Carbon powder	PTFE/C-15 s	PTFE/C-20 s	PTFE/C-25 s	PTFE/C-30 s
PTFE loading (%)	0	36.8	27.9	16.7	14.8
BET surface area (m^2/g)	232.6	50.8	101.2	142.2	161.2

150 mL deionized water and stirred. Next, PTFE (5 wt%) emulsion in deionized water (120 mL) was mixed together with Vulcan XC-72 carbon black dispersion. Then, water was evaporated from the solution and a nominal 60 wt% PTFE/C mixture was irradiated three times with cycles of 15–30 s microwaves on and 90 s microwaves off in order to decompose the surfactant in the PTFE emulsion and maintain the hydrophobicity of PTFE.

The particle diameters were in the range of 10–50 nm and were homogenously distributed in the fabricated PTFE/C nanocomposite. Moreover, compared with conventional methods, additional high temperature treatment and mechanical milling under liquid nitrogen frozen conditions were avoided (Table 6). The PTFE/C nanocomposite was then mixed with Pt/C/Nafion to obtain a Pt/C/Nafion-PTFE/C electrocatalyst, which resulted in enhancement of the mass transportation of Pt electrocatalyst without any adverse effect on the electrochemical activity.

The power output of the cell with a Pt/C/Nafion-PTFE/C nanocomposite cathode was 0.66 W/cm^2, which is 32% higher than that obtained for the cell with a standard Pt/C/Nafion cathode [73].

The microwave-assisted fabrication of Nafion 212/TiO_2 hybrid electrolytes for proton exchange membrane fuel cells (PEMFCs) operating at high temperature was also reported [74]. Nafion membranes dried at 110°C for 24 h were immersed in absolute ethanol with various concentrations of titanium tetraisopropoxide (TIP)

Table 7 Water and methanol uptake for different membranes

Substrate	Water uptake (%)	Methanol (2M) uptake (%)
Nafion	10.06	9.90
Nafion/tetraisopropoxide (TIP) 5%	13.35	9.56
Nafion/TIP 7%	14.40	8.80
Nafion/TIP 9%	17.77	7.91

precursor (5, 7, and 9% of TIP). To promote the formation of the Ti-peroxy sol, hydrogen peroxide was added and the membranes in solution mixtures were irradiated at different microwave power levels. Finally, the produced membranes were exhaustively treated with H_2SO_4 (0.5 mol/L) and distilled water at 70°C to remove residues. It was found that the samples comprised a mixture of Nafion and TiO_2 anatase phase, that the crystalline TiO_2 nanoparticles were inserted in the hydrophilic sites, and that Nafion acts as a template for the inorganic phase. Moreover, the roughness value of pure Nafion membrane measured by atom force microscopy (AFM) was around 0.559 mm and increased to 0.6301 and 1.087 mm for hybrid Nafion with 5 and 7% TIP, respectively. The hybrid Nafion/TiO_2 membranes showed a significant increase (10–30°C) in T_g of the polymers.

The hybrid membranes showed lower methanol absorption with increased amounts of TIP in the hybrid Nafion composites, which was a result of structure modification and higher crystallinity (Table 7). It was concluded that doping of nanosized inorganic oxide nanoparticles improved interconnection of ionic clusters in the polymeric matrix by providing a preferential pathway for proton hopping, thus enhancing proton conductivity. The results of electrochemical impedance spectroscopy (EIS) and solvent uptake measurements suggested enhancement of the hybrid membrane performance.

Microwave irradiation was also applied for in situ conversion of titania particles into titanate one-dimensional (1D) nanofilaments such as nanotubes and nanorods in a polymer Nafion matrix [75]. As a result, novel Nafion–titanate nanotube/nanorod composites for high-temperature direct ethanol fuel cells (DEFCs) were fabricated. In the first step, spherical nanoparticles of titania anatase were homogeneously dispersed into the conducting phase of Nafion using an in-situ sol–gel process. Then, titania particles were transferred in situ to titanate 1D nanofilaments by a microwave-assisted alkaline hydrothermal reaction. The process was carried out in a Teflon-covered stainless steel reactor placed in microwave oven at 140°C for 180 min (Fig. 22).

DEFCs based on Nafion–titanate hybrid electrolyte showed a significant enhancement of approximately 70% of the maximum power density compared with DEFCs using commercial Nafion without inorganic nanofilaments. It was also demonstrated that Nafion–titanate hybrid materials have enhanced mechanical stability at high temperature (∼130°C). This phenomenon was correlated with an effective interaction between organic and inorganic phases, which resulted in composite electrolytes with enhanced electrical and mechanical properties and reduced ethanol crossover [75].

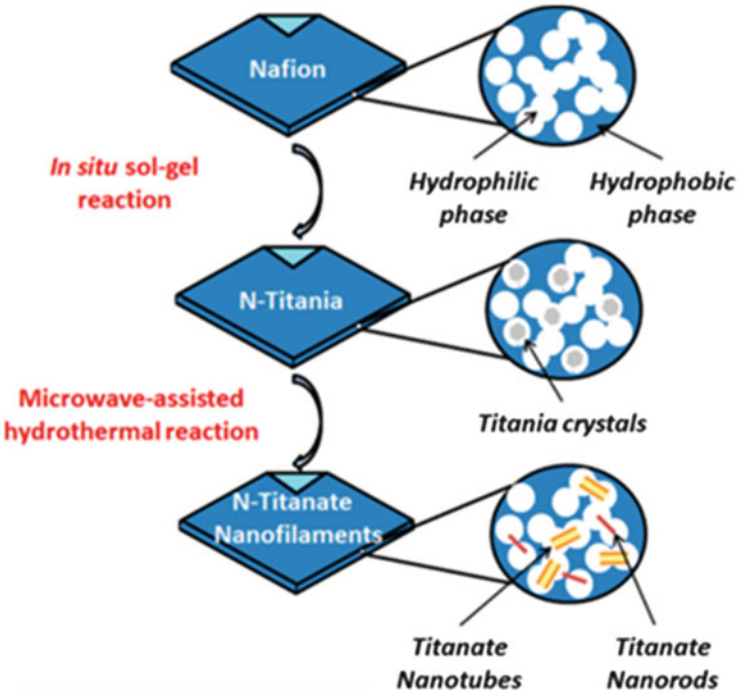

Fig. 22 Synthetic route for the preparation of Nafion–titanate nanotube/nanorod hybrids (Reprinted from [75] with permission)

3.8 Cellulose and Chitosan

Microwave irradiation was applied during the deposition of noble metals on CNTs wrapped with carboxymethyl cellulose (CMC) [76]. Carbon nanotubes such as single- (SWCNTs) and multiwalled (MWCNTs) nanotubes, and buckminsterfullerene (C-60) were well dispersed using the sodium salt of CMC, and then the addition of noble metal salts generated noble metal-decorated CNT composites at room temperature. For this process, 50 mg of CNTs (SWCNTs, MWCNTs, or C-60) were dispersed in 4 mL of 3 wt% CMC (sodium salt) by sonicating for 3 h. To this dispersion, 4 mL of noble salts such as $Na_2PtCl_6 \cdot 6H_2O$ (0.01 N), $HAuCl_4 \cdot 3H_2O$ (0.01 N), $AgNO_3$ (0.1 N), and $PdCl_2$ (0.1 N) were added and irradiated in a microwave reactor, maintaining the temperature at 100°C for 5 min. Similar control reactions were carried out without microwave irradiation. The average size of the Ag particles was 50 nm, and longer reaction times caused the formation of larger Ag clusters on SWCNTs, MWCNTs, and C-60. This indicates rapid nucleation of the particles on nanotubes, which took an initial 30 s, followed by particle growth [76].

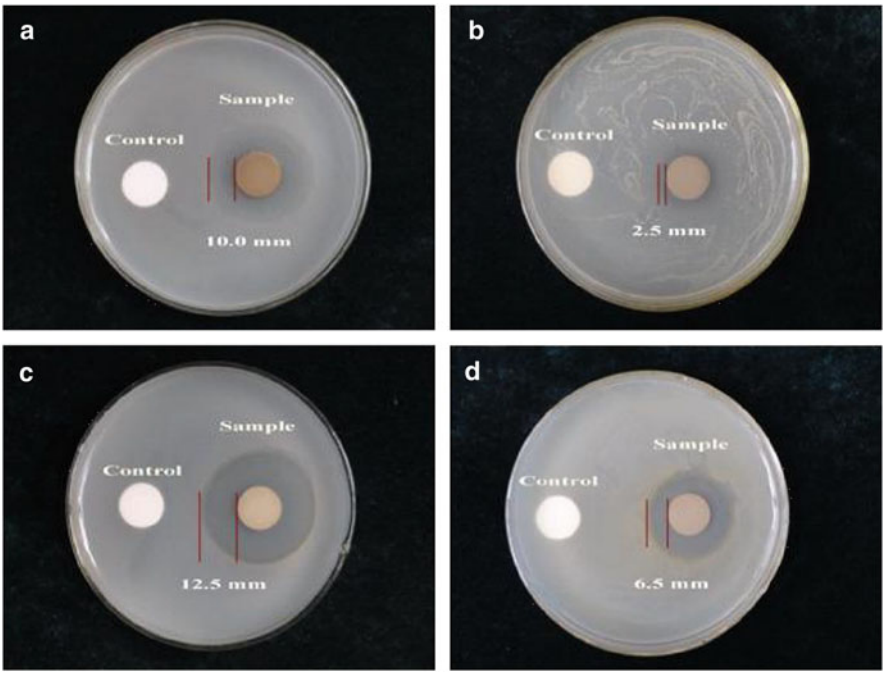

Fig. 23 Antimicrobial activity of cellulose/Ag nanocomposites against (**a, c**) *Escherichia coli* and (**b, d**) *Staphylococcus aureus*. Amounts of cellulose/Ag composite used were (**a**, **b**) 0.075 and (**c**, **d**) 0.150 g (Reprinted from [77] with permission)

More recently, a number of reports have been published on the modification of cellulose and the fabrication of composites containing nanoparticles, particularly AgNPs, which exhibit antimicrobial activity [77]. For example, such materials were prepared from microcrystalline cellulose (MC, 1.000 g) and $AgNO_3$ (0.340 g), which were vigorously stirred with ethylene glycol (50 mL) to form a uniform dispersed suspension. Then, the mixture was irradiated in a microwave reactor and kept at a certain temperature for 10, 30, and 60 min. The product was filtered, washed with ethanol, and dried under vacuum. SEM images showed that there were no significant differences in the morphology of the cellulose/Ag nanocomposites obtained under microwave irradiation at 140°C for 10, 30, and 60 min. Cellulose has a flake-like morphology and the silver particles with diameters of about 100 nm were homogeneously dispersed. Similarly, maintaining the reaction temperature (i.e., 140, 160, and 180°C) for 30 min only slightly influenced the structure and thermal stability of cellulose/Ag nanocomposites. The antibacterial activity of the cellulose/Ag nanocomposites was observed at low and high concentrations, i.e., 0.075 g (Fig. 23a, b) and 0.150 g (Fig. 23c, d) of cellulose/Ag nanocomposite.

The results showed that the cellulose/Ag nanocomposites had good antibacterial activity against both Gram-negative and Gram-positive bacteria, whereas MC does not have any antibacterial properties [77].

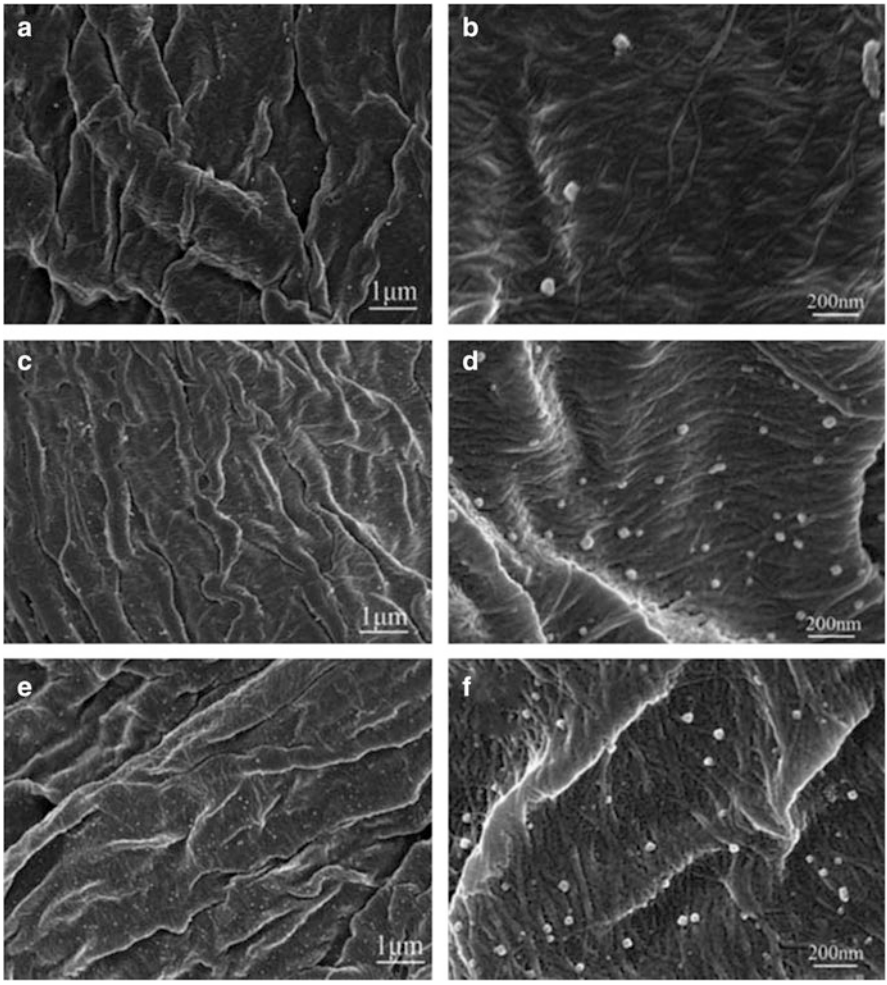

Fig. 24 SEM micrographs of cellulose/Ag nanocomposites prepared with different amounts of silver nitrate solution: (**a**, **b**) 5, (**c**, **d**) 10, and (**e**, **f**) 20 mL (Reprinted from [78] with permission)

Similarly, a simple and efficient microwave-assisted method was developed to synthesize cellulose/Ag nanocomposites by reducing silver nitrate in aqueous solution [78]. To obtain the nanocomposites, 0.1 g glucose and 0.1 g PVP were mixed together with a certain amount of distilled water, and 1.0 g cellulose fiber was added with vigorous stirring. Then, different volumes of 0.01 M $AgNO_3$ solution were added dropwise to the solution, which was then stirred for 15 min and irradiated in a microwave oven (560 W) for 10 min. SEM images showed that the AgNPs were well distributed on the surface of cellulose fiber and that the amount increased with increasing concentration of $AgNO_3$ (Fig. 24). In turn, high

amounts of PVP were conducive to the formation of spherical nanosilver particles with smaller size, but decreased the silver content of nanocomposites.

Compared with microwave irradiation, the composites obtained under conventional heating conditions had lower silver content, larger size, and darker color. Moreover, the antibacterial test results of cellulose Ag/nanocomposites demonstrated strong antimicrobial activity against both *Escherichia coli* (Gram-negative bacteria) and *Staphylococcus aureus* (Gram-positive bacteria).

Microwave irradiation was also applied for the preparation of jute cellulose fiber/Ag nanocomposites with carboxylate functional groups [79]. The oxidized jute sample was immersed in 0.015 M $AgNO_3$ solution and kept in the dark at ambient temperature for 12 h and thoroughly rinsed with deionized water. Finally, the suspension containing oxidized jute and $AgNO_3$ was irradiated in a microwave reactor for 5 and 10 min. It was found that the increase in reaction time from 5 to 10 min resulted in an increase in the average diameter of AgNPs from 50.0 ± 2.0 to 90.0 ± 4.7 nm; however, the crystallinity of the cellulose slightly decreased from 73.10 to 71.12%, respectively. Field effect SEM (FE-SEM) analysis showed that the AgNPs were uniformly distributed on the oxidized jute cellulose substrate and exhibited a small size and narrow size distribution (Fig. 25).

XRD showed that all the samples were composed of a mixed phase of crystalline cellulose type II and crystalline silver with a cubic structure, suggesting successful reduction of silver by cellulose–Na. The cellulose/Ag nanocomposites possessed high crystallinity, good thermal stability, and high surface area and can be used in green nanocomposites, ultrafiltration devices, antibacterial dressing, food packaging, water treatment, and biomedical applications [80].

Later, cellulose/Ag nanocomposites with antimicrobial activity were prepared by hydrothermal synthesis using $AgNO_3$ as Ag source and sulfated chitosan (molecular weight ~20,000 g/mol) as reducing and stabilizing agent [81]. Detailed comparison between composites fabricated by conventional heating and microwave irradiation was performed and a wide range of preparation parameters evaluated (i.e., reaction time and temperature, $AgNO_3$ to reducing agent ratio, and stirring speed). Microwave-assisted processes were carried out in a single-mode reactor equipped with magnetic stirrer and internal fiber-optic temperature probe. Based on the results, it was concluded that the heating method has only a minor influence on the final properties of the materials (e.g., silver content, nanoparticle effective diameter, and polydispersity). Additionally, the materials obtained both under conventional conditions and microwave irradiation showed excellent antimicrobial activity towards *E. coli*.

Microwave irradiation was also applied to obtain in one-step cellulose/AgCl nanocomposites characterized by homogeneous distribution of AgCl nanoparticles in the cellulose matrix [82]. Microcrystalline cellulose (MC, 1.416 g) and LiCl (1.510 g) were mixed with *N,N*-dimethylacetamide (DMAc, 20 mL) under vigorous stirring at 90°C for 3 h. The obtained cellulose solution (5 mL) was added directly to DMAc (30 mL), and then $AgNO_3$ (0.169 g) was added to the resulting solution under vigorous stirring. The solution was heated to 150°C under microwave irradiation. The resulting precipitate was separated from the solution by

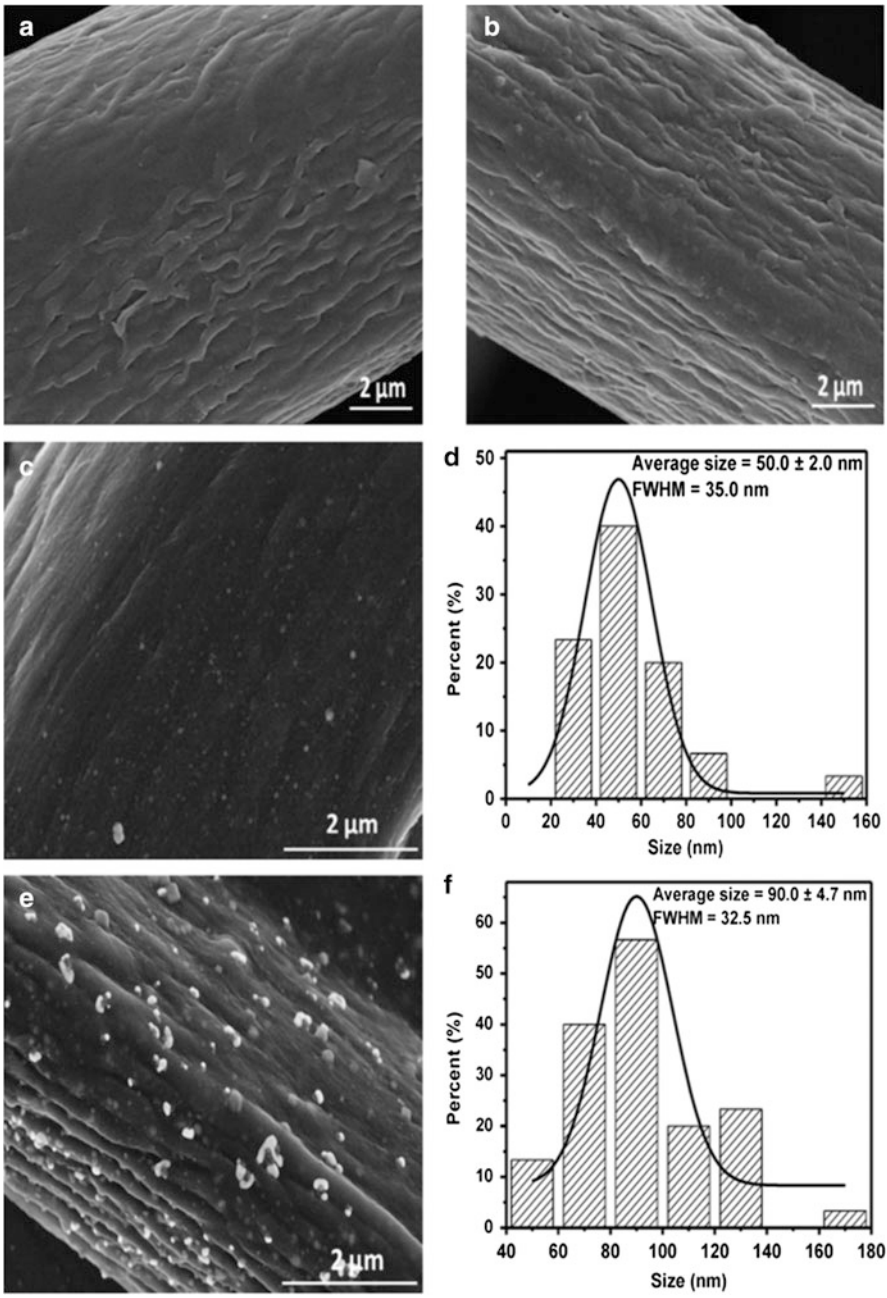

Fig. 25 FE-SEM images of (**a**) control jute fibers, (**b**) TEMPO oxidized jute fibers, (**c**) jute fibers with $AgNO_3$ after microwave heating for 5 min and (**e**) 10 min. (**d, f**) Particle size distribution of nanosilver on the jute fiber after microwave heating for 5 min (**d**) and 10 min (**f**); *FWHM* full width at half maximum (Reprinted from [80] with permission)

centrifugation, washed with water and ethanol several times, and dried at 60°C. The results of XRD analysis showed that all samples comprised a mixed phase of crystalline cellulose type I and well-crystallized AgCl with a cubic structure. The simultaneous formation of AgCl nanoparticles and precipitation of cellulose led to a homogeneous distribution of AgCl nanoparticles in the cellulose matrix. The cellulose/AgCl nanocomposites had good antibacterial activity against both Gram-negative and Gram-positive bacteria [82].

Similarly, applying ionic liquids, microwave protocols were developed for the preparation of cellulose/calcium silicate [83], cellulose/copper oxide [84], and cellulose/calcium carbonate [85] from $Ca(NO_3)_2{\cdot}4H_2O$ and $Na_2SiO_3{\cdot}9H_2O$, $CuCl_2{\cdot}2H_2O$, and $CaCl_2$ and Na_2CO_3, respectively. In the latter case, it was found that all samples had essentially no in vitro cytotoxicity and were comparable with the tissue culture plates.

The microwave-assisted route for the controlled synthesis of cellulose/hydroxyapatite (HA) nanocomposites from MC, $CaCl_2$, and NaH_2PO_4 in DMAc [86] as well as cellulose/fluorine-substituted HA nanocomposites from MC, $Ca(NO_3)_2{\cdot}4H_2O$, KH_2PO_4, and NaF in the presence of ionic liquids were developed [87]. In the typical protocol, the solutions of MC together with other components were heated under microwave irradiation to 150°C for 15, 20, and 30 min. The product was separated from the solution by centrifugation, washed with water and ethanol several times, and dried at 60°C. The XRD and SEM results indicated that HA nanostructures were synthesized in situ on the surface of cellulose and that the material consisted of cellulose and HA phase. TEM micrographs showed that the synthesized HA had a rod-like morphology and that the size of HA nanorods in the nanocomposites increased with increasing reaction time.

AgNPs were prepared in the presence of sodium citrate as a stabilizing agent by the in-situ reduction of $AgNO_3$ on acrylamide (AM) grafted onto bagasse paper sheets in order to develop a novel hybrid material for food packaging [88]. To activate the reactive sites, bagasse paper sheet was immersed in distilled water for 24 h. Then, AM together with potassium persulfate (KPS) were added to the reaction flask, which was irradiated in a microwave oven for 30 s to initiate the graft copolymerization of AM on the paper surface. The grafted paper sheet was treated with acetone, washed with methanol:water (80:20), and dried in vacuum at 40°C. In the next step, the sheet was put into $AgNO_3$ solution for 12 h and trisodium citrate solution for another 12 h to reduce Ag^+ ions into AgNPs, and then allowed to dry. Morphological studies of the paper sheet, grafted paper sheet, and AgNP-doped grafted paper sheet were performed by SEM. Sufficient deposition/polymerization of AM onto paper sheets was observed. The surface of the grafted sheet was extremely rough in comparison with the non-grafted fibers, which was attributed to the high graft density (Fig. 26).

Antibacterial activity studies showed that larger inhibition zones against both Gram-negative and Gram-positive bacteria were observed with AgNP-containing paper sheet than with untreated and grafted paper sheets (i.e., without AgNPs), which did not exhibit any antibacterial activity. Because the procedure does not

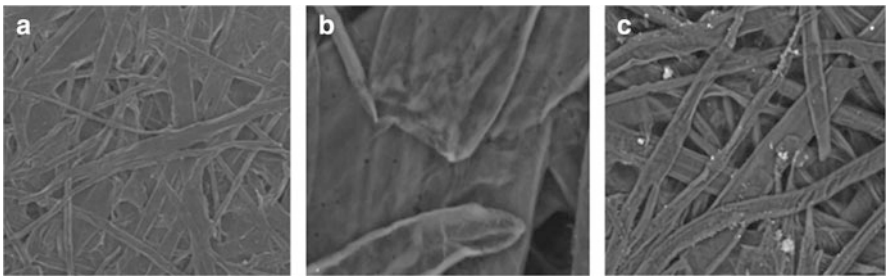

Fig. 26 Surfaces of (**a**) untreated paper sheet, (**b**) graft paper sheet, and (**c**) AgNP-containing paper sheet (Reprinted from [88] with permission)

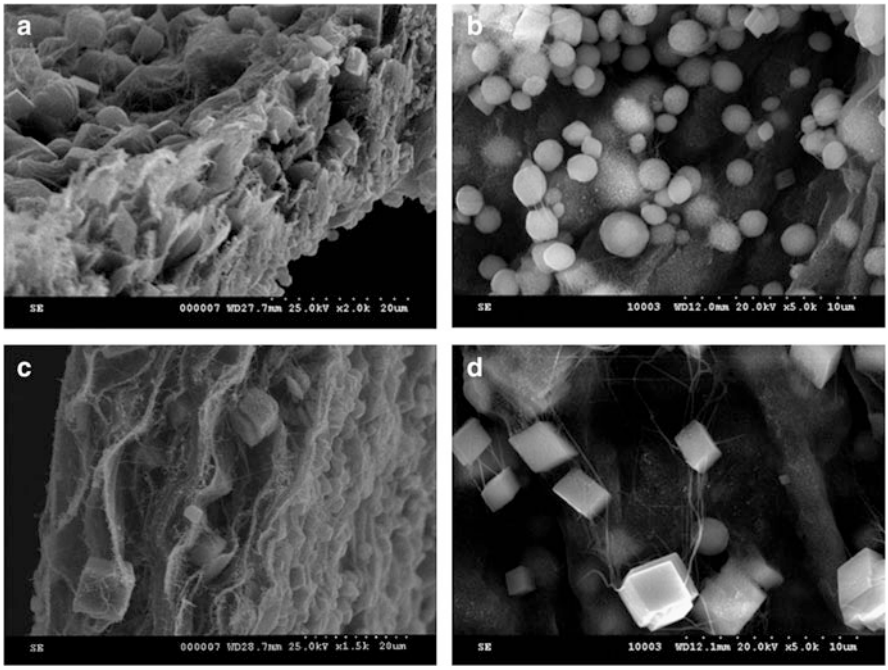

Fig. 27 Cross-section (**a**, **c**) and surface (**b**, **d**) SEM images of films F1R2 (MW exposure time 0 min., temp. 70°C) (**a**, **b**) and F12 (MW exposure time 5 min., temp. 70°C) (**c**, **d**) (Reprinted from [90] with permission)

involve organic solvents or harsh conditions, this method can be applied for the manufacture of antibacterial food packaging material.

Bacterial cellulose (BC), which is synthesized as nanofibrils by *Gluconacetobacter xylinus*, has been commercialized as diet food, filtration membranes, paper additives, and wound dressings [89]. BC can also be used in new functional material biocomposites that are suitable as implants in the tissue engineering of artificial skin, blood vessels, cartilage, and bone.

The formation of calcium carbonate crystals on BC membranes using microwave irradiation was investigated. The BC gel-like membranes were cut into rectangular (9 × 6.5 cm) strip samples (25 g wet BC) and immersed for 10 min in a beaker containing 50 mL of 0.1 M sodium carbonate. Afterwards, some of the samples were immersed in 50 mL calcium chloride solution and kept under microwave irradiation at 90 W for 3 or 5 min, the final measured temperatures in the solution being 50 and 70°C, respectively. Other samples, with the same weight but without microwave irradiation, were immersed for the same amount of time as the irradiated samples in 50 mL calcium chloride solutions at 50 and 70°C. Finally, the membranes were rinsed with deionized water and dried at room temperature.

It was found that the samples treated under microwave irradiation exhibited significantly different morphology and even polymorphism of the calcium carbonate crystals in comparison with those obtained in the absence of microwave irradiation. For all the irradiated samples, the $CaCO_3$ crystals were more uniform and their mean size was higher than those of the reference samples (Fig. 27) [90].

Synthesis of magnesium oxide (nano-Mg) chitosan-functionalized MWCNT composites, which are known for their antibacterial activity, was carried out under microwave conditions (Fig. 28). For this purpose, a mixture of 500 mg oxidized MWCNTs and chitosan solution (50 mg in 25 mL 2% acetic acid and 5 mL DMF) and 25 mg MgO were irradiated for 30 min in a microwave oven. Then, the reaction mixture was filtered, washed, and dried at 40°C under vacuum to obtain a composite material. SEM images indicated that a great amount of chitosan was attached to the MWCNTs. The attachment takes places not only at the tips but also at the side walls, with the thickness of the MWCNTs being about 10–15 nm, forming MWCNT–chitosan composites (Fig. 29). After nano-MgO grafting, the external surface roughness increased, whereas the tubular morphology of the

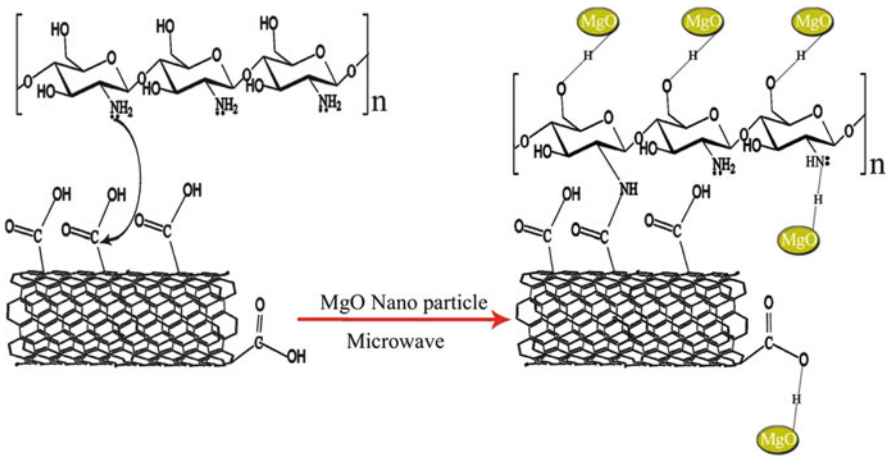

Fig. 28 Reaction scheme for the preparation of magnesium oxide chitosan-functionalized multiwalled carbon nanotube composites (MWCNT–chitosan–MgO) (Reprinted from [91] with permission)

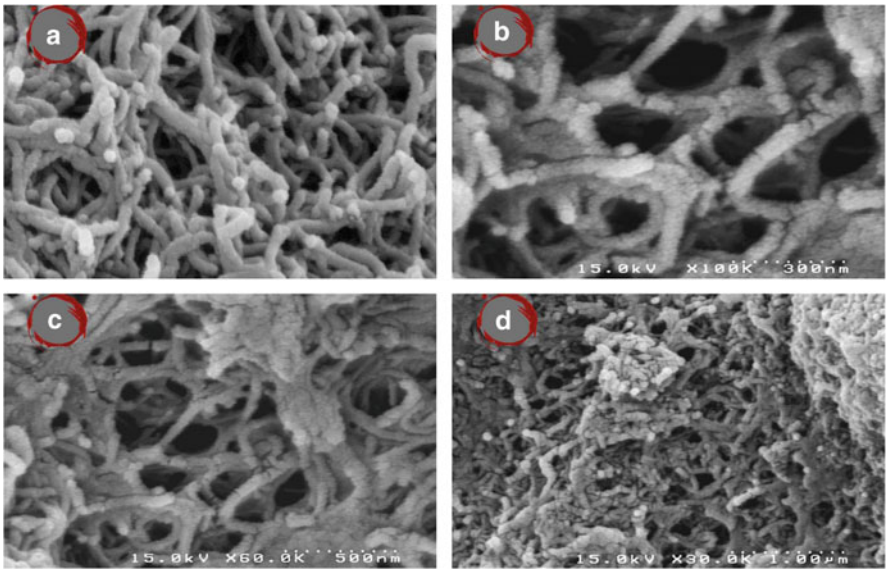

Fig. 29 SEM images of (**a**) oxidized MWCNTs and (**b–d**) MWCNT–chitosan–MgO composites (Reprinted from [91] with permission)

individual nanotubes was retained. Moreover, the MgO nanoparticles were attached to the whole surface of MWCNT–chitosan composites [91].

In a similar approach, the surface of chitosan-functionalized MWCNTs was modified using 2-hydroxyethyl methacrylate (HEMA) in a two-step procedure. First, a mixture of 200 mg initial MWCNTs and 10 mL of 70% HNO_3 was sonicated (40 min) and then irradiated in a microwave oven (30 min) to afford oxidized MWCNTs (MWCNT-COOH). At the second step, a mixture of 100 mg of oxidized MWCNTs and chitosan solution (0.1 g chitosan in 5 L 2% acetic acid and 5 mL DMF) was treated for 30 min with microwave irradiation. Then, the mixture was filtered, washed, and dried at 40°C under vacuum. In SEM images of the HEMA–chitosan–MWCNT composite, it was observed that the smooth MWCNT-COOH surface changed to a rough surface in the HEMA–chitosan–MWCNT composites. Moreover, the thickness of the HEMA–chitosan–MWCNT composite was increased to 35–40 nm. These morphological observations demonstrated successful graft of chitosan and HEMA monomers onto the side wall and tips of MWCNTs. A special advantage of this composite was the surface of modified chitosan, which allows bonding to other organic molecules that are able to perform polymerization reactions [92].

In order to intensify the chemical properties of lignin and chitosan that make them suitable for electrochemical application [93], the sol–gel method of preparation of chitosan/silica and lignin/silica hybrids was applied [79]. The composites were fabricated by irradiation of a water-methanol solution of chitosan or lignin at appropriate pH with addition of an alkoxysilane in a microwave reactor at 200 W

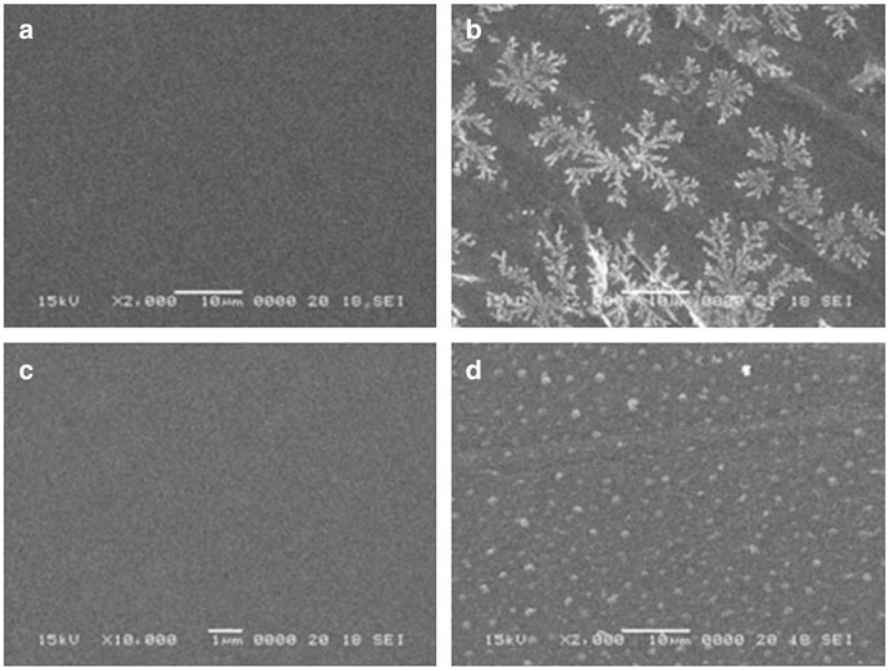

Fig. 30 SEM images of biopolymer/silica hybrids: (**a**) chitosan, microwave irradiation; (**b**) chitosan, conventional heating; (**c**) lignin, microwave irradiation; (**d**) lignin, conventional heating (Reprinted from [79] with permission)

for 20 min. In contrast, complete preparation of the composites under conventional heating at 60°C required more than 2 h, indicating that the rates of the sol–gel reactions were enhanced under microwave conditions compared with conventional heating. Moreover, application of the microwave-assisted method yielded completely homogenous nanoscale hybrids (Fig. 30a, c), whereas the silica composites prepared by conventional heating showed microheterogeneity (Fig. 30b, d). Thermostability of the biopolymer/silica hybrids and the porosity were almost the same, independently of the preparation method used.

A novel chitosan/ZSM molecular sieve composite used for the removal of Cu (II) ions from aqueous solution was prepared under microwave irradiation, applying a mixture of 0.5 g chitosan in 50 mL of 2% acetic acid to a ZSM molecular sieve. Then, 20% glutaraldehyde solution was added to the solution and the mixture irradiated for 3 min to crosslink the chitosan/ZSM composite. Composites with different ZSM contents and different crosslinker amounts were prepared. It was observed that introduction of ZSM improved the capacity for adsorption of Cu (II) ions in comparison with crosslinked chitosan. Finally, the effect of the amount of glutaraldehyde on Cu(II) adsorption was investigated and showed that the uptake of Cu(II) on chitosan/ZSM first increased and then decreased when the amount of crosslinker increased. The increase in Cu(II) adsorption was mainly attributed to the

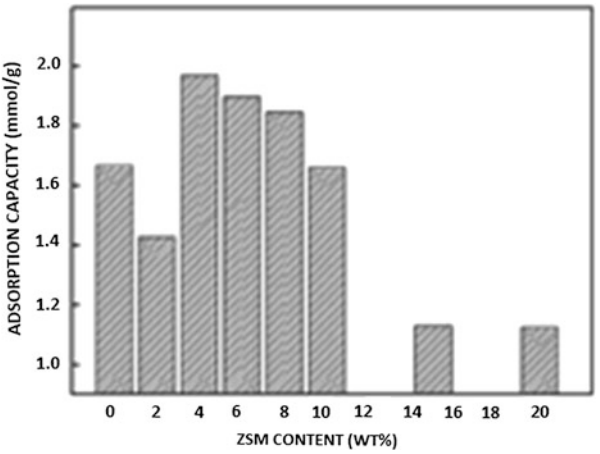

Fig. 31 Effect of ZSM content of a chitosan/ZSM molecular sieve on Cu (II) adsorption (Reprinted from [94] with permission)

low levels of crosslinking agent in the complex, which prevented the formation of closely packed chain arrangements (Fig. 31) [94].

Superabsorbent nanocomposites, which are hydrophilic polymers with the ability to absorb, swell, and retain large quantities of aqueous liquids, were prepared via both microwave and conventional techniques from guar gum grafted sodium acrylate (GG-*g*-NaA). During the reaction procedure, a mixture of guar gum (1.00 g) and sodium acrylate (2 g) in distilled water (100 mL) was kept to form a colloidal slurry. Then, 4 mL of an aqueous solution of APS (100 mg) as initiator and *N,N′*-methylenebisacrylamide (MBA) (95 mg) as crosslinker were added, and the mixture irradiated at 70°C with 800 W of microwave power for 2–15 min. For comparison, the mixture was also heated by the conventional method. The reaction parameters of both techniques were optimized and the microwave-assisted method was proved to have higher grafting yield with shorter reaction time (2–15 min) compared with the conventional method (10–60 min). The effect of crosslinker concentration on water absorbency was investigated to show that the addition of Cloisite®30B clay to the grafted material enhanced the swelling properties in all media, indicating its potential use in various applications, especially for dye removal (Table 8) [95].

Similarly, poly(acrylamide-aniline)-grafted gum ghatti [Gg-cl-poly (AM-aniline)]-based crosslinked conducting hydrogel, which can be applied for the manufacture of fuel cells, supercapacitors, and dye-sensitized solar cells, was prepared via a two-step synthesis method [96]. The first step involved microwave-assisted synthesis of a semi-interpenetrating (semi-IPN) polymer network based on acrylamide and gum ghatti using MBA and APS as a crosslinker–initiator system. In a typical experiment, 0.5 g gum ghatti was dissolved in 10 mL of water and calculated amounts of APS and MBA were added followed by dropwise addition of acrylamide under continuous stirring. The reaction mixture was irradiated with 850 W of microwave power for a fixed time and the product, Gg-cl-poly(AM), was

Table 8 Optimization of time of grafing reaction of sodium acrylate to guar gum for conventional and microwave condition

Time (min)	Grafting (%)
Conventional conditions	
10	3.7
20	3.8
30	5.8
40	6.5
45	3.7
50	3.7
55	8.6
60	8.8
Microwave irradiation	
2	2.75
4	2.95
6	2.98
8	5.59
10	11.12
15	8.92

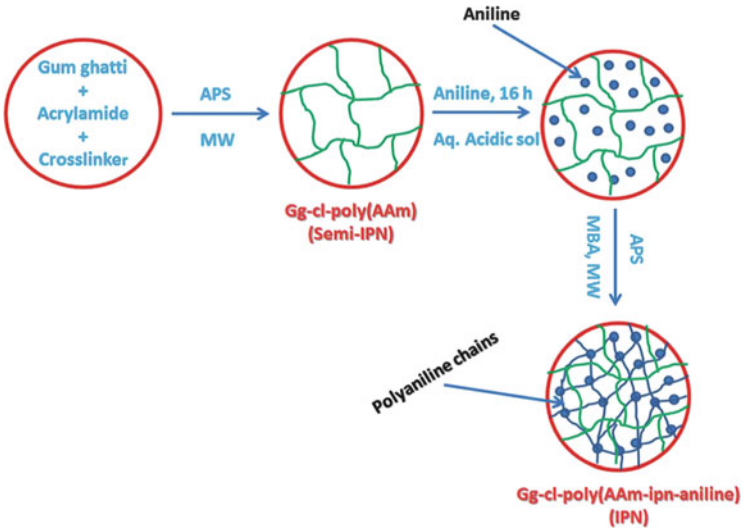

Fig. 32 Synthesis of hydrogel based on poly(acrylamide-aniline)-grafted gum ghatti [Gg-cl-poly (AAm-ipn-aniline)]; *IPN* interpenetrating network (Reprinted from [96] with permission)

separated from homopolymer through solvent extraction using acetone. Then, Gg-cl-poly(AM-aniline) was prepared by treatment of Gg-cl-poly(AM) with aniline in 0.5 N aqueous hydrochloric solution (Fig. 32).

It was found that the prepared hydrogels were conductive and that the current–voltage characteristics for various concentrations of HCl-doped Gg-cl-poly

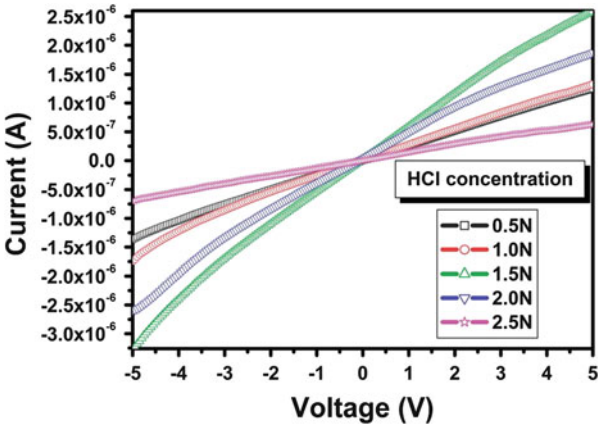

Fig. 33 Current–voltage characteristics for various concentration of HCl-doped Gg-cl-poly(AAm-ipn-aniline) (Reprinted from [96] with permission)

(AM-aniline) were of linear nature and obeyed Ohm's law. The conductivity was first enhanced with an increase in HCl concentration, and then decreased gradually when HCl concentration was excessive (Fig. 33).

3.9 Other

Magnetic nanoparticles are applied in such fields as cell isolation, targeted drug delivery, protein and enzyme immobilization, immunoassays, and environmental and food analyses because of easy separation of particles in an external magnetic field. Monodisperse magnetic Fe_3O_4/poly(styrene-*co*-acrylamide) [Fe_3O_4/poly (ST-*co*-AM)] nanoparticles were obtained by an emulsion polymerization of styrene and acrylamide monomers. The polymerization reactions were run in an aqueous solution of well-dispersed magnetic fluid solution (wt% $= 5.6 \times 10^{-2}$ g/mL), which was prepared by treatment of the reaction mixture in an ultrasonic bath for 3 min prior to polymerization, then 8.2×10^{-3} M KPS solution was mixed with the magnetic fluid solution. Finally, the styrene and acrylamide mixture was added to the magnetic fluid solution and irradiated at 75°C by 130 W of microwave power for 3 h. The resulting monodisperse magnetic particles were separated by repeated magnetic separation [97].

In comparison with magnetic nanospheres prepared under conventional conditions, TEM revealed that magnetic Fe_3O_4/poly(ST-*co*-AM) microspheres obtained under microwave conditions were characterized by smaller average size and more uniform distribution. Moreover, the average size of the magnetic Fe_3O_4/poly (ST-*co*-AM) nanoparticles increased together with the initial styrene and acrylamide concentrations and decreased with higher magnetic fluid concentration, which was caused by surfactant effects (Fig. 34) [97].

During the investigations on MWCNTs incorporated into poly(propylene) (PP) together with HA it was shown that microwave techniques could be

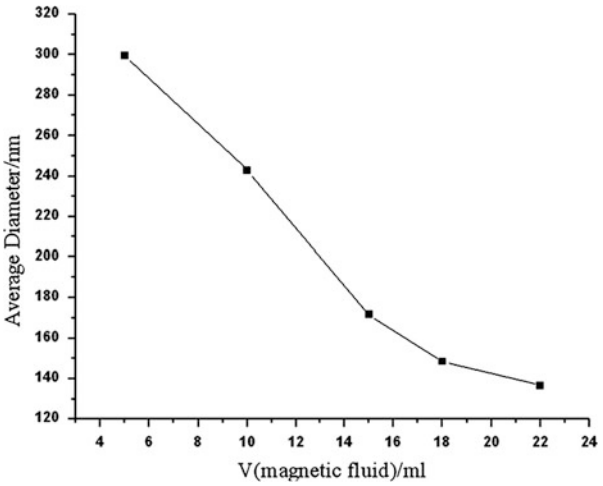

Fig. 34 Effects of ferrofluid content on the average particle diameter of magnetic Fe_2O_3/poly (styrene-*co*-acrylamide) microspheres (Reprinted from [97] with permission)

successfully applied for the faster processing of PP/MWCNT/HA biocomposites for bone tissue engineering [98]. Compared with conventional polymeric material processing methods, the heating time of PP/MWCNT/HA synthesis was significantly reduced to less than 1 min. In this study, MWCNTs were used as filler to improve the susceptibility for microwave absorption of the polymer during processing. The microwave-assisted synthesis of PP/MWCNT/HA with contents of PP (wt%) to MWCNTs (wt%) to HA (wt%) of 100:1:0, 100:1:5, 100:1:15, and 100:1:30 was carried out in a microwave reactor at 1,100 W of microwave power. The sintering time of each sample was measured. It was observed that the sintering time decreased with an increase in MWCNT and HA content. As expected, the incorporation of MWCNTs into the PP matrix improved the microwave energy absorption of the composites and consequently reduced sintering time. Moreover, SEM characterization of PP/MWCNT/HA nanocomposites demonstrated very uniform distribution of HA particles within the composites (Fig. 35). Additionally, it was observed that the composites with higher HA content (100:1:15) had the smallest pores and higher storage moduli [98].

Preparation and characterization of poly(amide-imide) (PAI) composites containing *p*-aminophenol (AP)-functionalized MWCNTs has been described [99]. Microwave irradiation was applied for the chemical functionalization of MWCNTs and synthesis of polymer matrix (Fig. 36). Amidation of carboxylated MWCNTs by AP was carried out in *N*,*N*-dimethylacetamide dispersion at 120°C for 15 min in a microwave oven with an output power of 700 W. PAI was synthesized by microwave-assisted polycondensation of 3,5-diamino-*N*-(4-hydroxyphenyl)benzamide (diamine) and *N*-trimetyllitylimido-L-isoleucine (diacid) in the presence of triphenyl phosphite as a catalyst; molten tetrabutylammonium bromide (TBAB) was applied as reaction medium. It was found that the melted salt strongly absorbs microwave energy and after only 8 min of irradiation at 130°C the polymer was obtained at 88% isolated yield. Finally, the

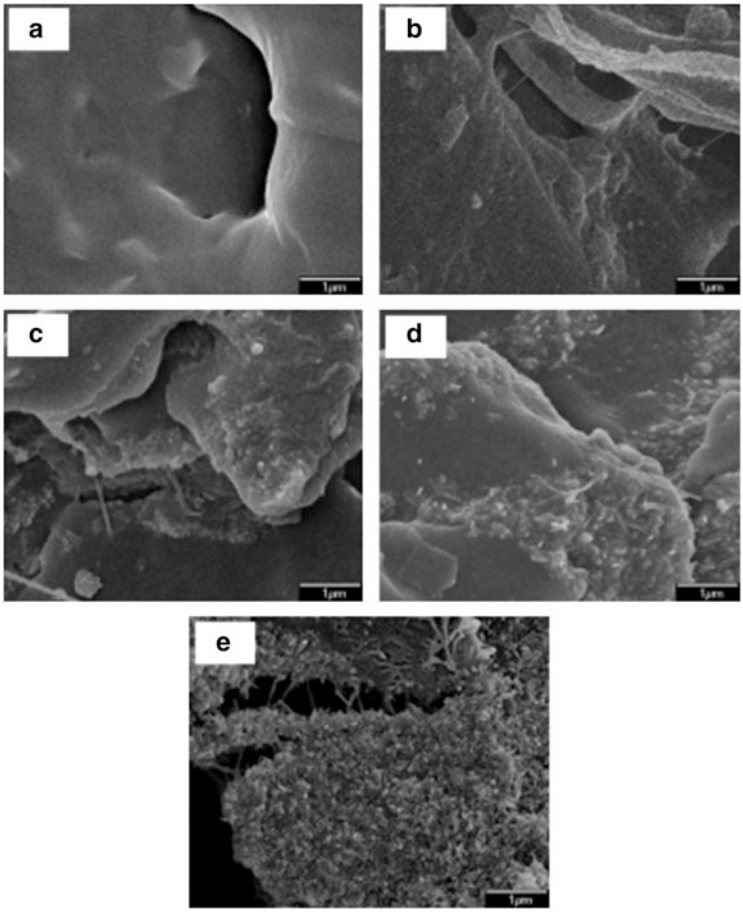

Fig. 35 FE-SEM images of the fractured surfaces of (**a**) unfilled PP, and sintered PP/MWCNT/HA composites of (**b**) 100:1:0, (**c**) 100:1:5, (**d**) 100:1:15, and (**e**) 100:1:30 composition (Reprinted from [98] with permission)

MWCNT–AP/PAI nanocomposites were prepared by step-drying of films with the nanofiller (5, 10, 15 wt%) dispersed in a *N,N*-dimethylacetamide solution of PAI. Incorporation of MWCNT–AP in the PAI matrix improved both the thermal resistance and mechanical properties of the material.

The microwave procedure was also used for preparation of exfoliated graphite/phenolic resin composites [100]. In the first stage, graphite flakes were intercalated by treatment with oxidizing mixture ($KMnO_4$/$HClO_4$/acetic anhydride) followed by microwave irradiation (domestic oven, 600 W for 50 s) to obtain exfoliated graphite (with high volume of ~500 mL/g). The exfoliated graphite /phenolic resin composites with various amounts (20–80 wt%) of exfoliated graphite filler were prepared by compression molding at room temperature using *p*-toluenesulfonic acid as crosslinking catalyst. It was found by electrical conductivity, microstructure, and

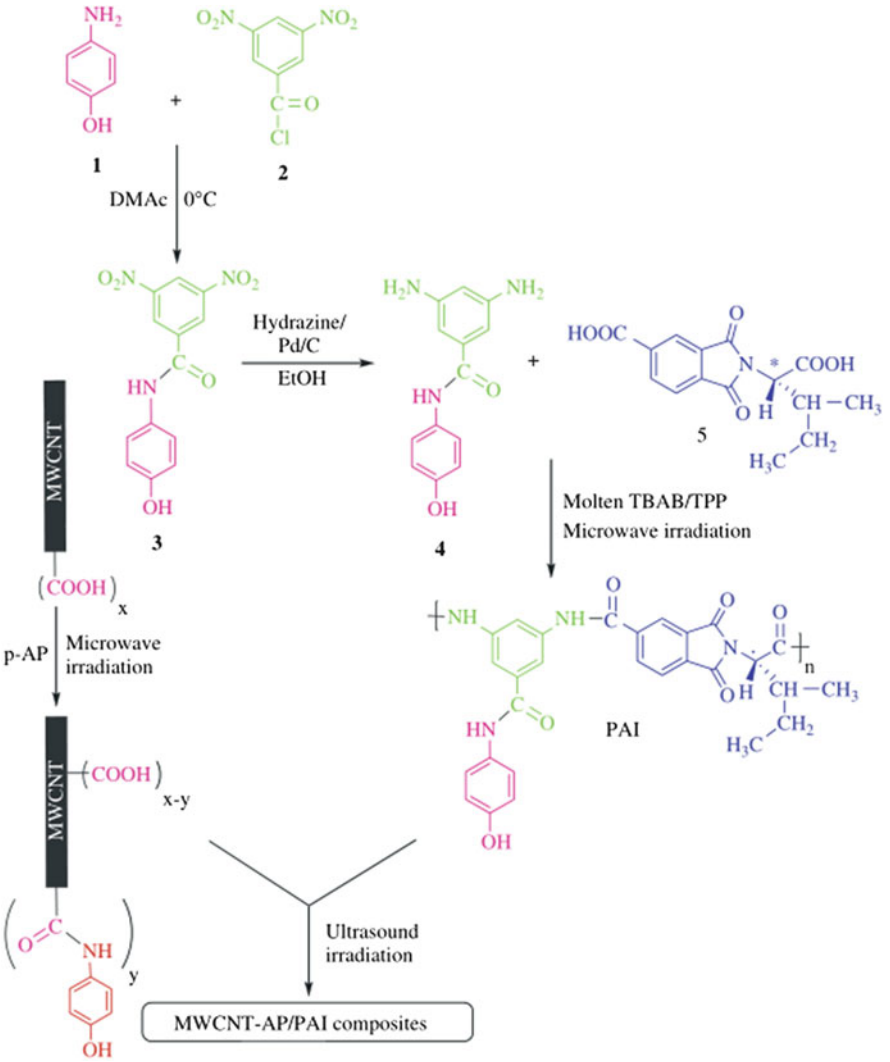

Fig. 36 Preparation of MWCNT–AP and MWCNT–AP/PAI composites (Reprinted from [99] with permission)

porosity studies in connection with TGA that addition of 50 wt% of exfoliated graphite is sufficient to obtain composites that fulfill requirements for materials for fabrication of bipolar plates in polymer electrolyte membrane fuel cells.

Microwave irradiation was successfully applied for grafting of polyamidoamine (PAMAM) dendrimers on silica [101]. The silica was treated under microwave irradiation with a 10% solution of γ-aminopropyltriethoxysilane (APTES) in toluene at 50°C for 10 min. The APTES-modified silica (Si-G0) was washed with MeOH and dried at 50°C. Then, grafting of PAMAM to Si-G0 surface was carried

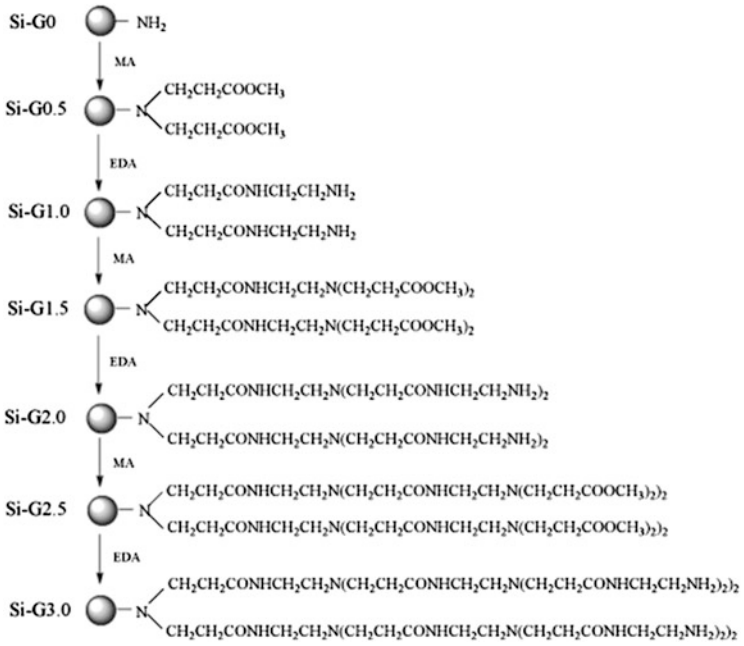

Fig. 37 Process of PAMAM grafting to silica (Reprinted from [101] with permission)

out in two steps: Michael addition of methyl acrylate to amino groups (Si-G0.5) followed by amidation of the resulting esters with ethylenediamine (EDA) (Si-G1.0), which were carried out in a microwave reactor at 40°C for 40 and 60 min, respectively. Then, Michael addition and the amidation reaction were repeated to graft further generations of dendrimer to the silica surface (Fig. 37).

Because PAMAM is highly fluorescent and fluorescence microscopy showed that the fluorescence intensity increased with increasing PAMAM generation, it can be assumed that PAMAM grew on the silica surface from the amino groups, whose content on the surface was also determined by titration (Fig. 38)

The reaction times under microwave irradiation and conventional heating conditions were compared. Conventional synthesis of Si-G0, Si-G0.5, and Si-G1.0 required 8, 24, and 24 h, respectively. Under microwave conditions, the reaction times were dramatically reduced to 10, 40, and 60 min, respectively.

Similarly, polycinnamamide (PCMA) Mg/Al mixed oxide nanocomposites (Fig. 39) obtained by a microwave-assisted process were found to be effective adsorbents of arsenate from aqueous medium [102]. The preparation route of PCMA hybrid nanocomposites consisted of several intermediate stages: polymerization of cinnamamide, synthesis of Mg/Al LDH, calcination of Mg/Al LDH into Mg/Al mixed oxide, and finally the coupling reaction of polycinnamamide gel with Mg/Al mixed oxide. The polymerization step and final coupling reaction were carried out in a microwave oven for several hours.

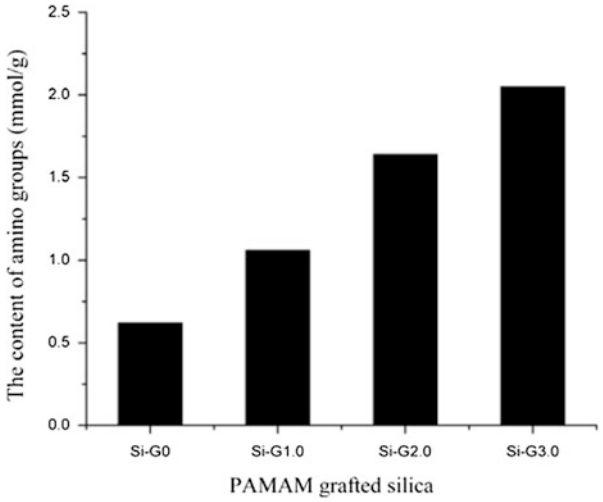

Fig. 38 Content of amino groups introduced onto the silica surface during PAMAM grafting. See Fig. 37 for description of grafted silicas (Reprinted from [101] with permission)

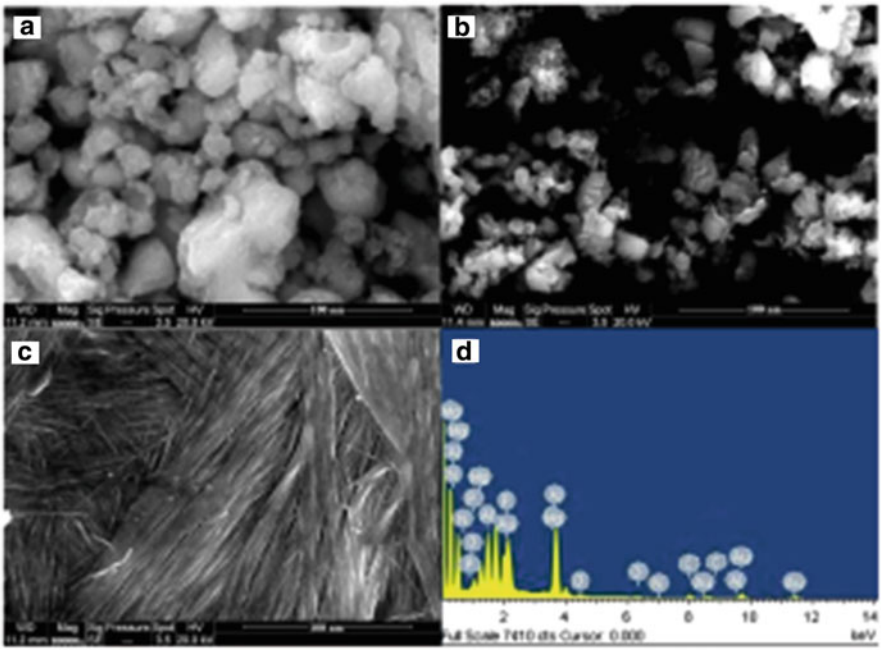

Fig. 39 SEM images of (**a**) Mg/Al carbonate LDH, (**b**) calcined LDH, and (**c**) polycinnamamide Mg/Al mixed oxide nanocomposite. (**d**) Energy dispersive X-ray (EDX) spectrograph of polycinnamamide Mg/Al mixed oxide nanocomposite (Reprinted from [102] with permission)

The absorbent properties of as-prepared PCMA nanocomposites were studied with respect to the effect of various parameters such as contact time, pH (6–12), initial arsenate concentration (1–50 mg/L), interfering anions, etc. The adsorption process was well fitted by a pseudo-second-order kinetic model and the maximum adsorption capacity calculated from Langmuir isotherm model was about 11.54 mg/g at 25°C [102].

Comparative studies on the properties of benzoxazine-based resins based on BPA and bio-based humic acid (containing naturally ~38% of inorganic minerals) prepared under microwave and conventional heating have been described [103]. First, benzoxazine precursors were prepared by reaction of phenolic compound (i.e., BPA or humic acid) with paraformaldehyde and aniline under solvent-free conventional (110°C, 60 min) or microwave-assisted (120°C, 5 min) conditions. Next, xylene solutions of the precursors were heated at 130°C for 96 h and, finally, the obtained resins were step-cured at 160, 180, and 200°C for 1–2 h. Generally, application of microwave irradiation did not influence the chemical structure (FTIR), thermal resistance (TGA), or microstructure (XRD) of obtained materials. The only discrepancy was noticed for the glass transition (T_g) of BPA-derived resins (DSC), probably caused by differences in the crosslink densities of prepolymers used.

The preparation of colloids with polymer core and inorganic shell consisting of AgNPs applied as building blocks for the manufacture of conducting composite films was reported [104]. The polymer colloids were prepared by copolymerization of styrene, butyl acrylate, 2-carboxyethyl acrylate (CA), and acetoacetoxyethyl methacrylate (AAEM) under microwave irradiation. The hydrophilic monomers CA and AAEM were used to introduce carboxylic and β-diketone groups into the surface layer of polymer colloids because they are able to complex metals and support growth of AgNPs on the polymer surface. The hydrophobic monomers styrene and butyl acrylate were used to form the core of polymer particles so that film formation was achieved at low temperatures. Then, hybrid particles were prepared by stirring polymer colloid (27 mL of 0.2 wt%) with silver salt solution (0.5 mL) for 30 min at room temperature. The reducing agent sodium hypophosphite was then added and the reaction mixture (5 mL) was irradiated in pressurized vessels for 2–5 min at various temperatures. The mixture was dialyzed against water for 3 days to remove substrates and by-products.

It was found that the content of AgNPs in composite samples was increased from 2 to 18 wt% when the reaction temperature increased from 80 to 120°C. Moreover, flow-field-flow-fractionation (F-FFF) experimental data showed that the formation of an inorganic shell around the polymer core took place only if synthesis was carried out at 120°C (Fig. 40). At lower reaction temperatures, secondary AgNPs and AgNP aggregates were detected as well as hybrid colloids.

It was also possible to prepare composite films with high electrical conductivity when AgNP loading on the polymer particle surface was above 20 wt%; the maximum loading of AgNPs on the polymer particle surface was 60 wt%. The application of hybrid colloids as building blocks for the formation of conducting films was feasible because of a combination of film-forming and conducting

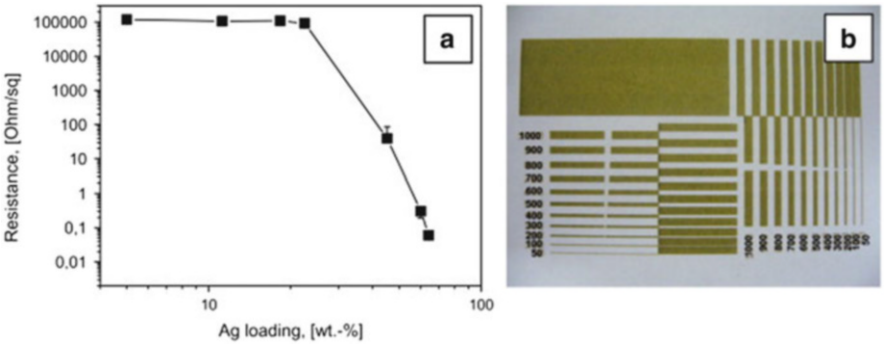

Fig. 40 (**a**) Conductivity of composite films as a function of the AgNP content. (**b**) Array prepared by ink-jet printing of hybrid colloids containing 18.3 wt% AgNPs on paper substrate (the *numbers* near each line indicate the width of the line) (Reprinted from [104] with permission)

components in a colloid form that can be used as ink in jet-printers for printing conducting elements in low-cost electronics for textiles or packaging (Fig. 40).

4 Summary

In summary, the application of microwave irradiation in the preparation of polymer hybrid materials and composites has been an attractive research field over the last two decades. The fabrication of polymer hybrid materials and composites faces considerable research challenges because their properties depend on proper molecular modeling and structural control of components in order to gain synergistic effects and improved properties of materials. It was shown that control of such parameters as particle size, particle size distribution, and particle density in a deterministic way under microwave irradiation strongly influences the properties of these materials. As the structural configuration of components moves away from its ideal configuration, the material properties stay in the same range as those of traditional microcomposites.

Despite the progress presented in this chapter, there are still a number of considerable research challenges within this field that need to be solved in order to explore the real advantages of hybrid materials and composites over traditional composite materials. A comparison of conventional and microwave curing brings a new momentum when the temperature distribution inside the material is considered, and that is where the research capabilities should be found. Different mechanics of heat generation and transfer under conventional and microwave conditions mean that microwave energy, in contrast to conventional heating, is supplied directly to a large volume of material, thus avoiding the thermal lags associated with conduction and/or convection mechanisms. Consequently, temperature gradients and thermal runaway caused by exothermic reactions during polymerization

can be reduced by precise control of microwave power and/or pulsed on-off irradiation cycles. In large composite structures, high temperatures caused by exothermic reactions can lead to degradation of the material and lowering of the mechanical properties. Thus, by applying pulsed microwave irradiation, it is possible to process the materials at higher temperatures and reduce processing time without thermal degradation compared with conventional processing.

References

1. Bogdal D, Prociak A, Michalowski S (2011) Curr Org Chem 15:1782
2. Lečkov M, Prandzheva S (2009) Encyclopedia of polymer composites: properties, performance and applications. Nova Science, New York
3. Matras-Postolek K, Bogdal D (2010) Adv Polym Sci 230:221
4. Skompska M (2010) Synth Met 160:1
5. Mandal B, Bhattacharjee H, Mittal N et al (2013) Nanomed NBM 9:474
6. Ge J, Neofytou E, Lei J et al (2012) Small 8:3573
7. Roach P, McGarvey DJ, Lees MR, Hoskins C (2013) Int J Mol Sci 14:8585
8. Iwasaki N, Kasahara Y, Yamane S et al (2011) Polymer 3:100
9. Yuan J, Gaponik N, Eychmüller A (2012) Anal Chem 84:5047
10. Prakash S, Chakrabarty T, Singh AK, Shahi VK (2013) Biosens Bioelectron 41:43
11. Krasia-Christoforou T, Georgiou TK (2013) J Mater Chem B 1:3002–3025
12. Mok H, Park TG (2012) Macromol Biosci 12:40
13. Shu JY, Panganiban B, Xu T (2013) Annu Rev Phys Chem 64:631
14. Work WJ, Horie K, Hess M, Stepto RFT (2004) Pure Appl Chem 76:1985
15. Gómez-Romero P, Sanchez C (2004) Functional hybrid materials. Wiley-VCH, Weinheim
16. Judeinstein P, Sanchez C (1996) J Mater Chem 6:511
17. Ávila-Orta CA, González-Morones P, Espinoza-González CJ et al (2013) Toward greener chemistry methods for preparation of hybrid polymer materials based on carbon nanotubes. In: Suzuki S (ed) Syntheses and applications of carbon nanotubes and their composites. InTech, Rijeka, p 167
18. Hussain F, Hojjati M, Okamoto M, Gorga RE (2006) J Compos Mater 40:1511
19. Fong H, Sarikaya M, White SN, Snead ML (2000) Mater Sci Eng C 7:119
20. Zaremba CM (1998) Chem Mater 10:3813
21. Bogdal D, Penczek P, Pielichowski J, Prociak A (2003) Adv Polym Sci 163:193
22. Wiesbrock F, Hoogenboom R, Schubert US (2004) Macromol Rapid Commun 25:1739
23. Hoogenboom R, Schubert US (2007) Macromol Rapid Commun 28:368
24. Bogdal D, Pisarek U (2012) Polymer chemistry under microwave irradiation. In: de la Hoz A, Loupy A (eds) Microwaves in organic synthesis. Wiley-VCH, Weinheim, p 1013
25. Bogdal D, Prociak A (2007) Microwave-enhanced polymer chemistry and technology. Blackwell, Ames
26. Hanemann T, Szabo DV (2010) Materials 3:3468
27. Zhang G, Niu A, Peng S, Jiang M, Tu Y, Li M, Ch W (2001) Acc Chem Res 34:249
28. Kojima Y, Usuki A, Kawasumi M et al (1993) J Mater Res 8:1185
29. Cao X, Lee LJ, Widya T, Macosko C (2005) Polymer 46:775
30. Thostenson ET, Chou T-W (1997) In: Proceedings of 12th annual meeting American Society for Composites, Dearborn
31. Thostenson ET, Chou T-W (2001) Polym Compos 22:197
32. Thostenson ET, Chou T-W (1998) In: Proceedings of the 13th annual meeting American Society for Composites, Baltimore

33. Liu Y, Xiao Y, Sun X, Scola DA (1999) J Appl Polym Sci 37:2391
34. Harper JF, Price DM (2005) In: 10th International conference on microwave and RF heating, Modena
35. Fang X, Scola DA (1999) J Polym Sci Part A Polym Chem 37:4616
36. Liu XQ, Wang YS, Zhu JH (2004) J Appl Polym Sci 94:994
37. Imholt TJ, Dyke CA, Hasslacher B et al (2003) Chem Mater 15:3969
38. Vázquez E, Prato M (2009) ACS Nano 3:3819
39. Ye Z, Deering WD, Krokhin A, Roberts JA (2006) Phys Rev B 74:75425
40. Xie R, Wang J, Yang Y et al (2011) Compos Sci Technol 72:85
41. Yang L, Li Z, Nie G, Zhang Z, Xiaofeng L, Wang C (2014) Appl Surf Sci 307:601
42. Chin IJ, Albrechta TT, Kima HC et al (2001) Polymer 42:5947
43. Jiankun L, Yucai K, Zongneng Q, Su YX (2001) J Polym Sci Part B Polym Phys 39:115
44. Yoo Y, Choi K-Y, Lee JH (2004) Macromol Chem Phys 205:1863
45. Aranda L, Mosqueda Y, Pérez-Cappe E, Ruiz-Hitzky E (2003) J Polym Sci Part B Polym Phys 41:3249
46. Urresti O, González A, Fernández-Berridi MJ et al (2011) J Membr Sci 373:173
47. Schmidt D, Sinha RS, Bousmina M (2005) Prog Mater Sci 50:962
48. Karaman VM, Privalko EG, Privalko VP et al (2005) Polymer 46:1943
49. Chen B, Evans JRG (2006) Macromolecules 39:747
50. Liao L, Zhang C, Gong S (2007) Macromol Rapid Commun 28:1148
51. Liao LQ, Liu LJ, Zhang C et al (2002) J Polym Sci Part A Polym Chem 40:1749
52. Liao L, Zhang C, Gong S (2007) Macromol Chem Phys 208:1301
53. Liao LQ, Liu LJ, Zhang C et al (2003) J Appl Polym Sci 90:2657
54. Wypych F, Satyanarayana KG (2004) Clay surfaces: fundamentals and applications. Elsevier, Amsterdam
55. Lee WD, Im SS (2007) J Polym Sci Part B Polym Phys 45:28
56. Martínez-Gallegos S, Herrero M, Rives V (2008) J Appl Polym Sci 109:1388
57. Uyanik N, Riza Erdem A, Fatih Can M, Çelik MS (2006) Polym Eng Sci 46:1104
58. Chang J, Liang G, Gu A et al (2012) Carbon 50:689
59. Pokharel P, Truong Q-T, Lee DS (2014) Compos Part B 64:187
60. Lin J-S, Chung M-H, Chen C-M et al (2011) J Phys Org Chem 24:193
61. Lin J-S, Chung M-H, Chen C-M et al (2010) Curr Appl Phys 10:1331
62. Wada Y (2007) Polymer 48:1441
63. Soumya S, Mohamed AP, Paul L, Mohan K, Ananthakumar S (2014) Sol Energy Mater Sol Cells 125:102
64. Chien W-C, Yu Y-Y, Chen P-K, Yu H-H (2011) Thin Solid Films 519:5274
65. Khan A, El-Toni AM, Alrokayan S et al (2011) Colloids Surf A 377:356
66. Sowntharya L, Subasrin R (2013) Ceram Int 39:4689
67. Yu Y-Y, Chen P-K (2013) Thin Solid Films 544:48
68. Tyliszczak B, Pielichowski K (2013) J Polym Res 20:191
69. He R, Qian X-F, Yin J et al (2003) Mater Lett 57:1351
70. Riaz U, Ashraf SM, Madan A (2014) New J Chem 38:4219
71. Riaz U, Ashraf SM, Kumar S, Ahmad I (2014) Chem Eng J 241:259
72. Riaz U, Ashraf SM (2012) J Phys Chem C 116:12366
73. Tian ZQ, Wang XL, Zhang HM et al (2006) Electrochem Commun 8:1158
74. Hammami R, Ahamed Z, Charradi K et al (2013) Int J Hydrogen Energy 38:11583
75. Matos BR, Isidoro RA, Santiago EI, Linardi M, Ferlauto AS, Tavares AC, Fonseca FC (2013) J Phys Chem 117:16863
76. Nadagouda MN, Varma RS (2008) Macromol Rapid Commun 29:155
77. Li S-M, Jia N, Ma M-G et al (2011) Carbohydr Polym 86:441
78. Xu Y, Zuo L, Lin T et al (2014) Polym Compos (in press) doi:10.1002/pc.23134
79. Kajiwara Y, Chujo Y (2011) Polym Bull 66:1039
80. Cao X, Ding B, Yu J, Al-Deyab SS (2013) Carbohydr Polym 92:571

81. Breitwieser D, Moghaddam MM, Spirk S et al (2013) Carbohydr Polym 94:677
82. Li S-M, Fu L-H, Ma M-G et al (2012) Biomass Bioenergy 47:516
83. Jia N, Li S-M, Ma M-G, Sun R-C (2011) Mater Lett 65:918
84. Ma M-G, Qing S-J, Li S-M et al (2013) Carbohydr Polym 91:162
85. Ma M-G, Dong Y-Y, Fu L-H et al (2013) Carbohydr Polym 92:1669
86. Ma M-G, Zhu J-F, Jia N et al (2010) Carbohydr Res 345:1046
87. Jia N, Li S-M, Ma M-G, Sun R-C (2012) Mater Lett 68:44
88. Kamel S (2012) Carbohydr Polym 90:1538
89. Lin S-P, Loira Calvar I, Catchmark JM et al (2013) Cellulose 20:2191
90. Stoica-Guzun A, Stroescu M, Jinga SI et al (2013) Ind Crop Prod 50:414
91. Shariatzadeh B, Moradi O (2014) Polym Compos 35:2050
92. Mahmoodian H, Moradi O (2014) Polym Compos 35:495
93. Jesionowski T, Klapiszewski Ł, Milczarek G (2014) J Mater Sci 49:1376
94. Li H, Huang D (2013) J Appl Polym Sci 129:86
95. Likhitha M, Sailaja RRN, Priyambika VS, Ravibabu MV (2014) Int J Biol Macromol 65:500
96. Sharma K, Kaith BS, Kumar V et al (2013) RSC Adv 3:25830
97. Huang J, Pen H, Xu Z, Yi C (2008) React Funct Polym 68:332
98. Chen L, Tang CY, Ku HS-l, Tsui CP, Chen X (2014) Compos Part B 56:504
99. Mallakpour S, Zadehnazari A (2014) Polym Int 63:1203
100. Sykam N, Gautam RK, Kar KK (2014) Polym Eng Sci (in press) doi:10.1002/pen.23959
101. Zhang C, Su P, Umar Farooq M et al (2010) React Funct Polym 70:129
102. Islam M, Mishra PC, Patel R (2013) Chem Eng J 230:48
103. İnan TY, Karaca BY, Dogan H (2012) J Appl Polym Sci 128:2046
104. Türke A, Fischer W-J, Adler H-J, Pich A (2010) Polymer 51:4706